RSC Advances

PAPER

View Article Online
View Journal | View Issue

Cite this: *RSC Adv.*, 2024, **14**, 39977

Rational design and synthesis of novel phenyltriazole derivatives targeting MRSA cell wall biosynthesis†

Mohamed M. Elsebaei, *[a] Hany G. Ezzat,[a] Ahmed M. Helal,[a] Mohamed H. El-Shershaby,[a] Mohammed S. Abdulrahman,[b] Moaz Alsedawy.,[b] Ahmed K. B. Aljohani, [c] Mohammed Almaghrabi,[c] Marwa Alsulaimany,[c] Basmah Almohaywi,[d] Read Alghamdi,[c] Samar F. Miski,[e] Arafa Musa[f] and Hany E. A. Ahmed *[a]

Received 14th October 2024
Accepted 2nd December 2024

DOI: 10.1039/d4ra07367c

rsc.li/rsc-advances

Antimicrobial resistance in methicillin-resistant *Staphylococcus aureus* (MRSA) is a major global health challenge. This study reports the design and synthesis of novel phenyltriazole derivatives as potential anti-MRSA agents. The new scaffold replaces the thiazole core with a 1,2,3-triazole ring, enhancing antimicrobial efficacy and physicochemical properties. A series of derivatives were synthesized and evaluated, with four compounds (**20**, **23**, **29** and **30**) showing significant activity against MRSA (MIC ≤ 4 μg mL^{-1}). Compound **29** emerged as the most promising candidate, showing rapid bactericidal activity and superior performance over vancomycin in time-kill assays. It exhibited selective toxicity against bacterial cells, minimal cytotoxicity in human cell lines and low hemolytic activity. Mechanistic studies showed that compound **29** targets the bacterial cell wall by binding to penicillin-binding protein 2a (PBP2a), disrupting cell wall integrity. Additionally, it showed strong anti-biofilm activity and reduced MRSA biofilms by up to 40%. Preliminary pharmacokinetic profiles suggested a favorable profile, including a prolonged plasma half-life and good oral bioavailability. These results suggest that compound **29** is a promising lead for further development in the fight against MRSA.

1. Introduction

Antimicrobial resistance poses a major public health risk worldwide.[1] Antibiotic-resistant infections, once considered a problem of the future, are now a familiar reality that kill tens of thousands of people every year. A prime example is methicillin-resistant *Staphylococcus aureus* (MRSA), which has become resistant to several antibacterial drugs.[2,3] MRSA infections are associated with high mortality rates and are challenging to treat. The emergence of bacteria resistant to multiple drugs raises the possibility of a post-antibiotic era in which there are inadequate treatment options and recurrent infections that can lead to death.[4,5] The consequence is enormous health and economic losses across the world, which is running out of its arsenal of antibacterial agents. According to a list published by the WHO, Gram-positive bacteria are considered a significant health risk, especially multidrug-resistant bacteria such as methicillin-resistant *Staphylococcus aureus* (M.R.S.A.).[6,7] Additionally, the Infectious Disease Society of America (I.D.S.A.) defines the E.S.K.A.P.E. pathogens (*Enterococcus faecium*, *Staphylococcus aureus*, *Klebsiella pneumonia*, *Acinetobacter baumannii*, *Pseudomonas aeruginosa* and *Enterobacter cloacae*) as posing a worldwide threat.[8] Therefore, new clues need to be found to defeat resistant enterobacteria without affecting the microbiota. As the number of antimicrobials decreases worldwide, everyone should have the responsibility to address antimicrobial resistance. In our laboratory, the search for a good antibacterial agent began with phenylthiazole, which was originally discovered as a thiazole core with a guanidine head and an alkyl chain end.[9–19] Recently, this scaffold has been intensively studied and optimized to improve its activity and metabolic profile. While the phenylthiazoles

[a]*Pharmaceutical Chemistry Department, Faculty of Pharmacy, Al-Azhar University, Nasr City 11884, Cairo, Egypt. E-mail: m.elsebaei@azhar.edu.eg; heahmad@azhar.edu.eg*

[b]*Microbiology and Immunology Department, Faculty of Pharmacy, Al-Azhar University, Nasr City 11884, Cairo, Egypt*

[c]*Pharmacognosy and Pharmaceutical Chemistry Department, Pharmacy College, Taibah University, Al-Madinah Al-Munawarah 41477, Saudi Arabia. E-mail: Akjohani@taibahu.edu.sa*

[d]*Department of Pharmaceutical Chemistry, College of Pharmacy, King Khalid University, Abha 61421, Saudi Arabia*

[e]*Department of Pharmacology and Toxicology, College of Pharmacy, Taibah University, Medina 42353, Saudi Arabia*

[f]*Department of Pharmacognosy, College of Pharmacy, Jouf University, Sakaka, Aljouf 72341, Saudi Arabia*

† Electronic supplementary information (ESI) available. See DOI: https://doi.org/10.1039/d4ra07367c

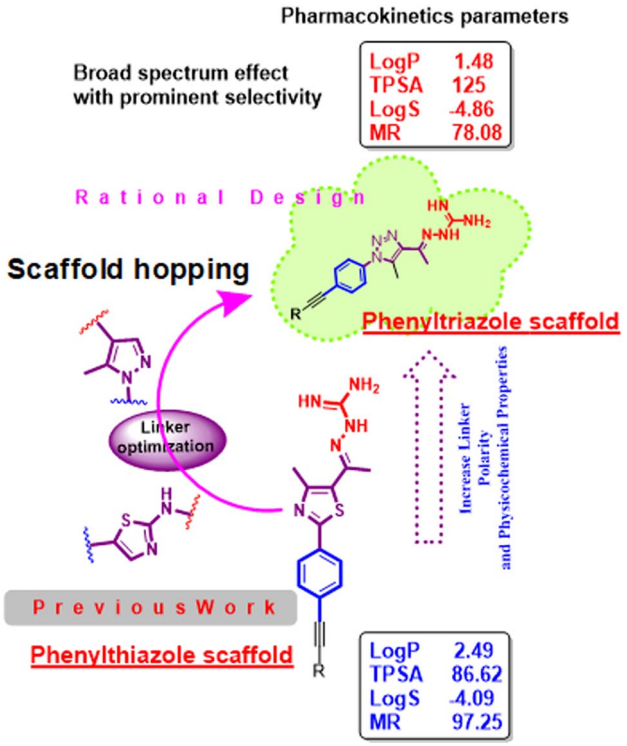

Fig. 1 Previous work and rational design of the triazole scaffold.

showed anti-biofilm activity, the poor permeability of phenylthiazole may play a role in its narrow spectrum. Therefore, a modification was made to the linker between the head and the scaffold. However, the solubility of the resulting product was not encouraging.[20–23] Then a modification to the tail gave us the second generation, which showed intracellular effectiveness.[24,25] However, the metabolic profile had to be improved by incorporation of a nitrogen atom in place of the active metabolite ($-CH_2$) to obtain the third generation as phenyltriazole (Fig. 1).

Therefore, this study attempts to modify the scaffold to explain its activity against a variety of microbial organisms and expand our knowledge on the structure–activity relationship of this new class of antimicrobial agents. The idea of the present scaffold is based on replacing the thiazole core with a 1,2,3-triazole ring, which is suggested to have antimicrobial activity against a variety of microorganisms and enhanced physicochemical properties. 1,2,3-Phenyltriazole derivatives have been extensively studied for their antibacterial and antifungal activities and DNA gyrase inhibitor has been proposed as a potential target for the development of antibacterial and antifungal agents. Many 1,2,3-triazoles have been shown to be effective and have several useful biological properties, such as antiviral,[26] antiepileptic,[27] antifungal,[28] antibacterial,[29] antimicrobial,[30] antiprotozoal,[31] antioxidant[32] and anticancer activities.[33] These 1,2,3-triazoles find their way into medicinal chemistry and form some drugs available on the markets. The most well-known structures (Fig. 2), include tazobactam (**A**),[34] cefatrizine (**B**),[35] rufinamide (**C**),[36] and carboxyamidotriazole (**D**).[37]

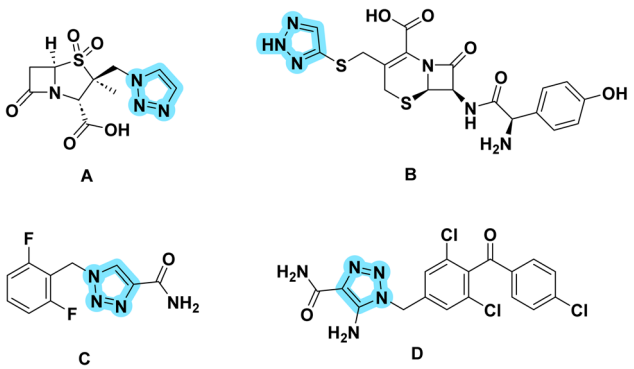

Fig. 2 Structures of some drugs containing the 1,2,3-triazole nucleus.

2. Results and discussion

2.1. Chemistry

In Scheme 1, the first step is to prepare the commercially expensive 1-azido-4-bromobenzene (**2**) (CAS number: 2101-88-4) by oxidation of readily available *p*-bromoaniline *via* diazotization, then treating with sodium azide to afford compound **2**. The latter was allowed to react with acetylacetone in the presence of sodium ethoxide to afford compound **4** as yellow crystals. According to the standard Sonogashira cross-coupling protocol, compound **4** was reacted with alkyne derivatives in the presence of copper(I) iodide as a catalyst, bis(triphenylphosphine)palladium(II) dichloride and triethylamine as a base, to afford compounds **5–16**. While compounds **17** and **18** were available as 4-bromotoluene and 3-bromothiophene, we first reacted ethynyltrimethyl silane with compound **4** *via* Sonogashira cross-coupling without using potassium carbonate to avoid deprotection of TMS (trimethyl silane), thereby yielding a byproduct using an excess of triethylamine as a base, and then deprotected the TMS using potassium carbonate in methanol to obtain the intermediate 1-(1-(4-ethynylphenyl)-5-methyl-1*H*-1,2,3-triazol-4-yl)ethan-1-one, which reacts with two aryl halides (4-bromotoluene and 3-bromothiophene) *via* typical Sonogashira cross-coupling to afford compounds **17** and **18**. Subsequently, the target compounds **19–32** were obtained by condensation of the phenyltriazole derivatives **5–18** with aminoguanidine hydrochloride (Scheme 1).

2.2. Biological screening

2.2.1 Antibacterial screening and SAR study. The assay for the antibacterial effect of the lead compounds, acetyl derivatives **5–18** showed very weak activity (MIC > 125 μg mL^{-1}) due to loss of the hydrophilic guanidine moiety, which was reported to be essential for activity.[24,25]. An initial screening of the newly prepared compounds **19–32** against MRSA USA300, one of the clinically important and highly pathogenic MDR pathogens,[38–40] revealed that only four derivatives (compounds **20**, **23**, **29** and **30**) have promising antibacterial activity (Table 1). The active derivatives have MIC values ≤ 4 μg mL^{-1}. The SAR of this new set of alkynylphenyltriazole analogues appeared to be very clear,

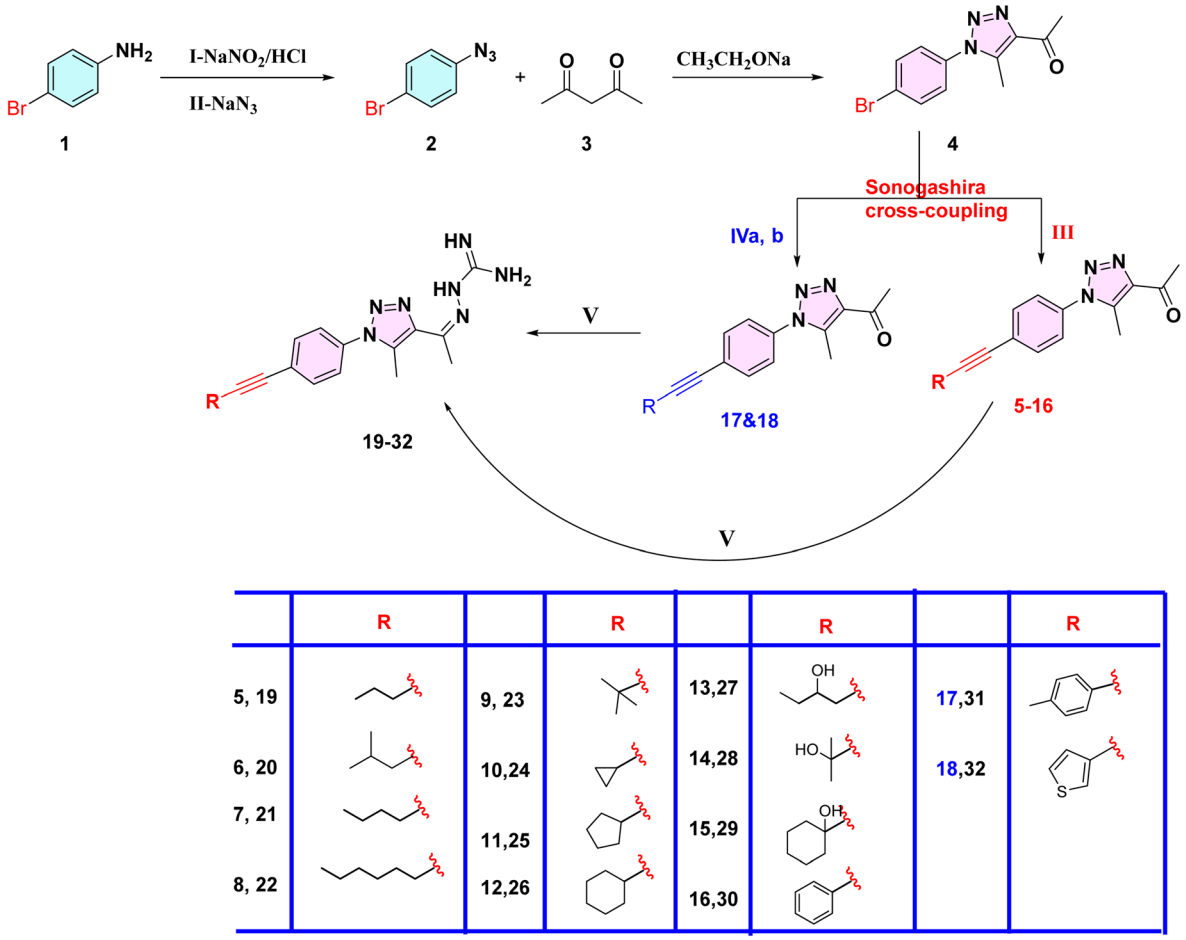

Scheme 1 Reagents and conditions: (I)$NaNO_2$/HCl and stirring at 0–5 °C for 30 min. (II) NaN_3 with stirring for 1 h at R. T. (III) $PdCh(PPH_3)_2$ (5% mol), CuI (7.5% mol), K_2CO_3 (2 equiv.), triethylamine, acetylene derivatives, DME, heat at 110 °C for 24 h comp. (**5–16**); (IV) (a) $PdCl_2(PPh_3)_2$ (5% mol), CuI (7.5% mol), Et_3N, DME, ethynyltrimethyl silane (2 eq.), at 50 °C for 2 h; (b) absolute MeOH, K_2CO_3, stirring for 1 h; (c) $PdCl_2(PPh_3)_2$ (5% mol), CuI (7.5% mol), K_2CO_3 (2 equiv.), Et_3N, DME, comp. (**17** & **18**) (1 eq.), at 110 °C for 6–24 h;(V) aminoguanidine HCl, EtOH, conc. HCl, heat to reflux, 3 h.

as the antibacterial activity was directly correlated with the terminal branched chain and terminal ring size. In this sense, the branched compounds **20** and **23** provided an active compound (MIC value of **20** and **23** is 4 μg mL^{-1}). While the ring size was increased to a six-membered ring, a potent compound with an MIC only four-fold higher than that of vancomycin was provided (the MICs of **29** and **30** are 4 μg mL^{-1} and the MIC of vancomycin is 1 μg mL; Table 1). Antimicrobial activity is abolished by reducing the ring size of the terminal cyclic alkynylphenyltriazole derivatives to five or three units. However, the compounds that were active against the TolC-mutant *E. coli* showed low activity (MIC values ≥ 64 μg mL^{-1}) against the wild type-strain.

The antibacterial evaluation was then expanded to include four additional Gram-positive and Gram-negative strains, including *Staphylococcus aureus* (ATCC 43300, clinical isolates), *Klebsiella pneumoniae* (ATCC 13883), and *Pseudomonas aeruginosa* (ATCC 10145) as Gram-negative bacteria.

In general, the synthesized compounds were more effective against Gram-positive microorganisms than against negative ones, as shown in (Fig. 3).

2.2.2 Time-kill assay. From Table 1, it can be shown that the MIC values of the most promising compounds were four fold higher than the corresponding MIC value of vancomycin, the drug of choice in the treatment of MRSA. To investigate whether these compounds are bactericidal or bacteriostatic, a time-kill assay was used (Fig. 4), which indicated that the most important compounds in this study were **29** and **30**. Both compounds surpassed the performance of vancomycin, the drug of choice for the treatment of staphylococcal infections in terms of the time required to exert its bactericidal effect against MRSA. Briefly, vancomycin, the standard control antibiotic, shows a gradual decline in the bacterial count over time, eventually reaching complete eradication after about 24 hours, while both compounds show potent bactericidal activity, rapidly reducing the MRSA count and achieving complete bacterial eradication within 24 hours, comparable to vancomycin (Fig. 4).

Overall, both compounds **29** and **30** exhibit potent and time-dependent bactericidal activity against MRSA, achieving complete eradication within 24 hours, with results comparable to those of vancomycin. This suggests that these phenyltriazole

Table 1 The minimum inhibitory concentrations (MIC in μg mL^{-1}) of the compounds initially screened against various clinical isolates[a]

Cp.	MRSA NRS384 (MRSA USA300)	*Clostridium difficile* ATCC BAA 1870	*E. coli* JW55031 (TolC mutant)	*Enterococcus faecalis* ATCC 51299	*Neisseria gonorrhoeae* 181	*C. albicans* SS5314 (wild type)	*Escherichia coli* BW25113 (wild type)
19	32	32	32	8	64	16	>64
20	**4**	8	8	8	32	8	>64
21	32	16	32	32	>64	16	>64
22	64	64	64	64	>64	64	>64
23	**4**	4	32	8	>32	4	>64
24	64	64	64	>64	>64	>64	>64
25	64	>64	64	>64	64	>64	>64
26	16	16	64	8	>64	16	>64
27	>64	>64	>64	>64	>64	>64	>64
28	16	16	64	16	>64	16	>64
29	**4**	8	8	8	64	4	>64
30	**4**	>64	16	16	>64	8	>64
31	**8**	2	4	8	>64	2	>64
32	16	32	32	>64	>64	32	>64
Linezolid	1	1	8	1	64	>64	NT
Vancomycin	1	1	16	64	>64	>64	NT
Gentamicin	NT	NT	0.25	NT	NT	NT	NT
Tetracycline	NT	NT	NT	NT	2	NT	NT
Fluconazole	NT	NT	NT	NT	NT	0.5	NT

[a] NT: Not tested.

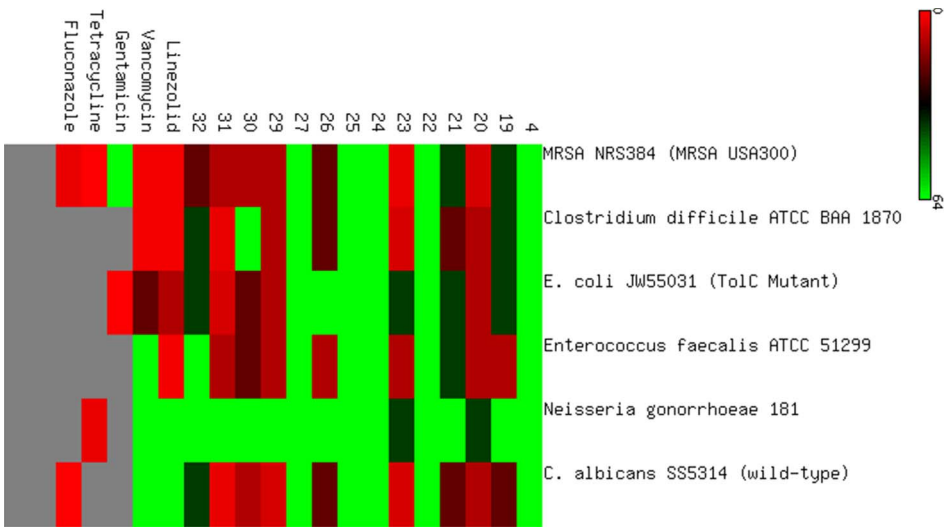

Fig. 3 Heatmap distribution of the antibacterial effect of target compounds against a panel of microbial strains.

derivatives are promising candidates for the treatment of MRSA infections.

2.2.3 Assessment of cytotoxicity. Selectivity toward prokaryotic cells is an essential feature of any antibiotic candidate. In this context, compound **29**, the most potent analogue, was observed in two human cell lines: Caco-2, the colorectal adenocarcinoma cell line and the W-I38, the diploid normal cell line. The results of these studies are presented in Table 2. The selectivity index (SI) in each cell line was the ratio of the IC_{50} value of cytotoxicity of a specific human cell line divided by the MIC values for specific bacterial strains. Compound **29** had good SIs of between 2 and 17.5 against MRSA, *Clostridium difficile* and *C. albicans* isolates compared to normal cells, suggesting that compound **29** is relatively safe for human cells and at the same time effective against pathogens. Furthermore, it showed low cytotoxicity against cancer cells with an SI of 0.69–11. Overall, the data suggest that compound **29** has strong antibacterial activity against MRSA, *C. difficile* and *C. albicans* with a high selectivity index, especially in the normal WI38 fibroblast cells, indicating a good therapeutic index. However, its potency and selectivity against *E. coli* and *N. gonorrhoeae* are significantly reduced,

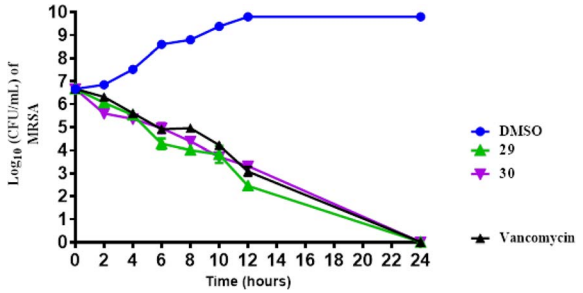

Fig. 4 Killing kinetics of selected phenyltriazole compounds (tested in triplicate at 4 × MIC) against methicillin-resistant *Staphylococcus aureus* over a 24 hours incubation period at 37 °C. DMSO (compound solvent) served as a negative control and vancomycin served as a control drug.

Table 2 Cytotoxicity of compound **29** in colorectal adenocarcinoma and normal human diploid fibroblasts

		Selectivity index[a]	
Organism type	MIC (μg mL^{-1})	Caco-2	WI38
MRSA NRS384 (MRSA USA300)	4	5.5	17.5
Clostridium difficile ATCC BAA 1870	4	5.5	17.55
E. coli JW55031 (TolC mutant)	32	0.69	2.194
Enterococcus faecalis ATCC 51299	8	2.75	8.775
Neisseria gonorrhoeae 181	32	0.69	2.194
C. albicans SS5314 (wild type)	4	5.5	17.55

[a] Selectivity index = IC_{50}/MIC. The IC_{50} values of compound **29** against both Caco-2 and W-I38 cells were 21.98 ± 1.12 and 70.2 ± 3.57 μg mL^{-1}, respectively. The IC_{50} value = the concentration that reduced Caco-2 or WI38 cell viability by 75%.

highlighting the variable activity of the compound for different pathogens.

2.2.4 Analysis of the effect of compound 29 on the morphology of MRSA cells. The general theoretical analysis of the mechanism of action of these analogues is based on their structure bearing variable lipophilic parts and terminal hydrophilic parts. The lipophilic systems favored attachment to the membrane because the lipophilicity favored the embedding of the compound into the cell. This embedding caused the compound to act as a false substrate for the target enzyme instead of glucosamine, resulting in cell wall inhibition. We hypothesized that the thicker peptidoglycan-rich Gram-positive cell wall was prevented more than the Gram-negative one and this was clear from the observed antimicrobial data. In addition, understanding the mechanism of action of antibacterial agents is crucial for their development and optimization. Compound **29** was investigated, and the rapid killing activity was indicative of the membrane targeting activities, which may be mediated by an electrostatic interaction between the positively charged central nitrogen atoms in compound **29** and other analogues as well as the negatively charged bacterial membrane. This hypothesis is consistent with the fact that positively charged antibacterial peptides can disrupt the integrity of the bacterial membrane and depolarize bacterial membranes.[41] To test this hypothesis, a microscope from Nikon Eclipse Ci, Japan was used to visualize the morphology of bacterial cells at high resolution providing direct evidence for the membrane effects caused by compound **29**. Fig. 5 serves to highlight the effect of compound **29** on the bacterial morphology. In Fig. 5A and C (untreated control), the cells are intact and show normal morphology, whereas in Fig. 5B and D (treated with compound **29**), the cells exhibit signs of structural damage, suggesting that compound **29** disrupts the bacterial cell wall, ultimately leading to cell death. This provides visual evidence for the antimicrobial mechanism of action of compound **29**, which likely targets essential components of bacterial cell wall biosynthesis.

2.2.5 Growth curve analysis. Methicillin-resistant *Staphylococcus aureus* (MRSA) represents a significant challenge in clinical settings due to its high drug resistance. To further validate the antibacterial mechanism of the novel phenyltriazole scaffold, MRSA was selected as a model organism for detailed studies. Growth curve analysis serves as a critical method to assess the effectiveness of compound **29** by tracking bacterial proliferation over time in treated *versus* untreated samples. In contrast to the bacteria treated with compound **29**, the results shown in Fig. 6 show that the number of bacteria not treated with compound **29** (DMSO) increased significantly. However, treatment with compound **29** resulted in a sharp decrease in the number of live bacteria that could be treated with either 2 × MIC or 4 × MIC concentrations, which were better than reference vancomycin. Accordingly, a wide concentration range of compound **29** and different incubation times were used, revealing that it has remarkable antibacterial potential.

2.2.6 Anti-biofilm effect. In the development of new antibiotics, the ability to inhibit bacterial virulence factors such as biofilm formation is a crucial property. Biofilms act as protective barriers to bacteria, shielding them from the effects of antibiotics and leading to persistent infections.[42] This makes treating biofilm-associated infections particularly challenging, especially in clinical environments where biofilms form on medical devices. Therefore, the development of antibacterial agents with effective anti-biofilm activity is crucial.[43,44] When compound **29** was tested for its ability to eradicate preformed, mature staphylococcal biofilm, it was found to be superior to ceftriaxone in eradicating MRSA biofilm, disrupting approximately 37% of the MRSA biofilm mass at 4 × MIC (Fig. 7). The most important compound in this series (compound **29**) showed the lowest biofilm eradication activity as it disrupted only 40% of the MRSA biofilm (Table 3).

2.2.7 Hemolytic activity. Before any pharmaceutical application, it is important to assess the safety profile of new drug candidates, particularly their potential to cause hemolysis, which may lead to toxic effects. Hemolytic activity refers to the breakdown of red blood cells and the release of hemoglobin, which can indicate toxicity to human cells. According to European Medicines Agency (EMA) guidelines, *in vitro* hemolysis studies are conducted to ensure the compatibility of new

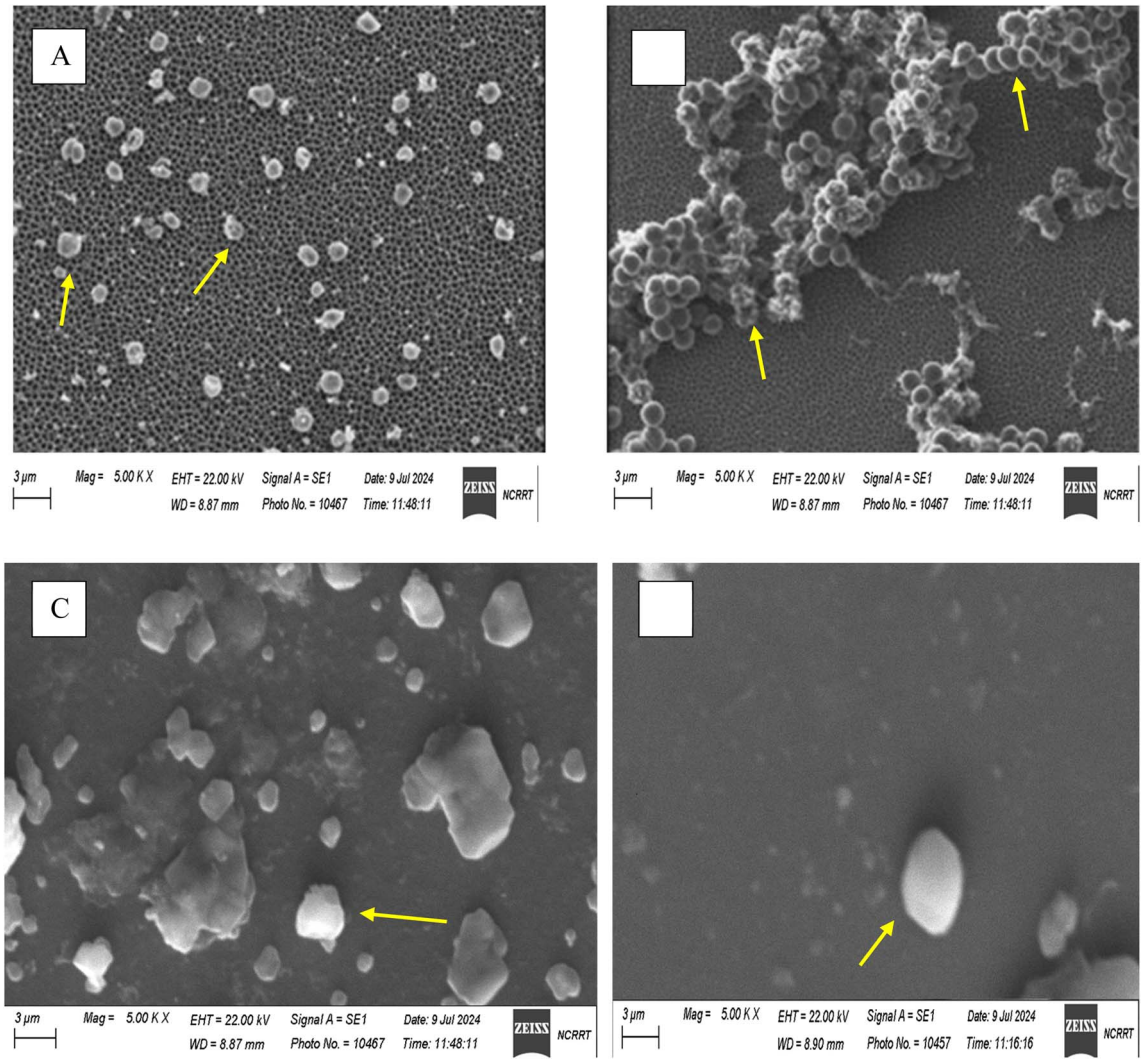

Fig. 5 Scanning electron microscope (SEM) photomicrographs of methicillin resistant *Staphylococcus aureus* cells. (A and C): Treated with 2 × MIC of analog **29**. The yellow arrows point to deformed *S. aureus* cells: irregular cell shapes and abnormally fused cells. (B and D): Untreated control cells.

compounds with human blood cells.[45] In this study, red blood cell lysis by hemoglobin release in plasma was evaluated for the representative potent **29** analogue and compared to ciprofloxacin as a positive control. The results showed a hemolytic activity of 15% of the drug ciprofloxacin in the studied MIC concentration range of up to 64 µg mL^{-1}. Furthermore, analog **29** did not show strong hemolytic activity against human

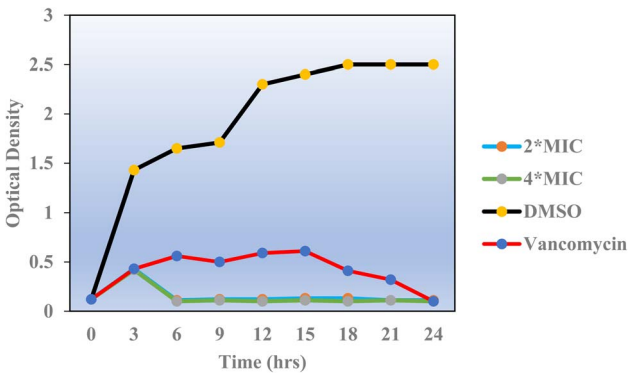

Fig. 6 The growth curve of the MRSA is affected by **29**. The results were considered significant at $p < 0.01$.

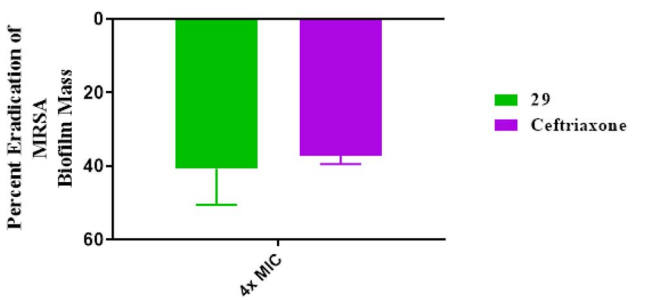

Fig. 7 Disruption of mature MRSA USA300 biofilm by the tested phenyltriazole and ceftriaxone (at 4 × MIC). The data are presented as percent disruption of MRSA mature biofilm.

Table 3 The antibiofilm data of the potent **29** analog against different microbial strains[a]

ID	Organism	IZD	MIC	MBC	T	Inhibition of biofilm formation (%)
29	MRSA ATCC 43300	33.34 ± 0.47	3.9	15.625	4	79.39 ± 0.37
	K. pneumonia ATCC 13883	28.67 ± 0.47	7.8	31.25	4	72.11 ± 0.51
	E. coli ATCC 25922	30.67 ± 0.47	3.9	31.25	8.01	65.43 ± 0.45
	C. albicans ATCC 10231	37.67 ± 0.47	7.8	31.25	4	75.29 ± 0.53
	P. aeruginosa ATCC 10145	21.67 ± 0.47	31.25	62.5	2	46.99 ± 0.66
Ceftriaxone	MRSA ATCC 43300	30.34 ± 1.24	8	8	1	73.262 ± 0.21
	K. pneumonia ATCC 13883	34.34 ± 0.47	4	8	2	61.23 ± 0.22
	E. coli ATCC 25922	36 ± 1.50	16	32	2	59.14 ± 0.16
	C. albicans ATCC 10231	37.67 ± 0.47	7.8	31.25	4	82.50 ± 0.14
	P. aeruginosa ATCC 10145	**35 ±1.85**	**8**	**16**	**2**	**74.39 ± 0.68**

[a] IZD: inhibition zone diameter expressed as mean number of millimeters ± SD, MIC: minimum inhibitory concentration; μg mL^{-1}, MBC: minimum inhibitory concentration; μg mL^{-1}, T = tolerance: MBC/MIC.

erythrocytes up to 64 μg mL^{-1}. Therefore, the novel scaffold is considered hemocompatible with a very low hemolytic activity up to 64 μg mL^{-1}. The hemocompatibility results are consistent with the cytotoxicity evaluation. Compound **29** showed low toxicity to Caco-2 and WI38 cells. This is better than the performance of the phenylthiazole scaffold with a hemolysis-dependent concentration mode, which has a reversed safety profile compared to that of phenyltriazole .[10,22,46–49]

2.3. Molecular docking of the PBP2a target

Antibiotic resistance has emerged in response to the overuse of currently available antibiotics.[50] Therefore, it is necessary to discover and develop novel antibacterial compounds with new formulations to combat severe infections.[51] MRSA infection is one of the most common causes of hospital-acquired disease and is currently associated with poor prognosis and increased mortality/morbidity.[15,22,46,47,49] The key factor in broad-spectrum β-lactam resistance in MRSA strains is penicillin-binding protein 2a (PBP2a). Due to its low affinity for β-lactams, PBP2a provides transpeptidase activity to enable cell wall synthesis at β-lactam concentrations that inhibit the β-lactam-sensitive PBPs normally produced by *S. aureus*. In the present study, molecular docking simulations were performed to identify the possible mechanism of such a novel phenyltriazole scaffold as a prominent cell wall disruptor of the active site of SauPBP2a. However, targeting the PBP2a allosteric site is another alternative strategy to reduce SauPBP2a activity. Therefore, we also evaluated the binding affinity of our potent analogs in PBP2a active site inhibitors including compound **29** and recorded binding data (Table 4). The crystal structure of PBP2a was considered, and the PDB code 1MWT was used for the experiments. All previous validation steps were performed, and re-docking of the bound ligand was performed. Interestingly, compound **29** exhibited high binding affinity to the active site of PBP2a with a $\Delta G_{binding}$ value of −7.39 kcal mol^{-1}.

2.4. Binding affinity analysis of penicillin-binding protein 2a

Penicillin-binding protein 2a (PBP2a) is an essential protein involved in the resistance of methicillin-resistant *Staphylococcus aureus* (MRSA) to β-lactam antibiotics and a potential antibacterial target.[52] PBP2a can also perform the function of transpeptidase, complete cell wall synthesis and maintain the growth and proliferation of bacteria, thereby exhibiting multi drug resistance.[53] Therefore, it is urgent to develop potential specific PBP2a inhibitors to overcome the multi drug resistance of MRSA to most current antibiotics. The binding affinity of potent analogs based on the inhibitory effect on MRSA and other microbial strains toward the PBP2a target was examined using inhibition constant data, and Ki is an effective parameter for cell wall destruction. The diagram in Fig. 8 shows the mode of action.

The dock scores of potent analogs **20**, **23**, **29**, **30**, and **31** are estimated and using an equation the inhibition constants, Ki, were calculated and compared (Table 5). The equation used for Ki calculation is as follows:

$$\mathrm{Ki} = \exp(\Delta G/(R \times T)),\ (T = 298\ \mathrm{K})$$

2.5. Pharmacokinetic profiling

One of the fundamental challenges of translating promising compounds from the bench to clinical trials is addressing the physicochemical limitations of a compound, with almost 90% of drugs currently in the drug discovery/development pipeline having poor physicochemical properties, such as limited aqueous solubility, poor permeability, or both.[54] Our earlier generation phenylthiazoles exhibited poor physicochemical profiles including limited ability to permeate the gastrointestinal tract, as evaluated *via* the Caco-2 bidirectional permeability assay. This was due in large part to the lead compound being a substrate for the P-gp efflux system.[55] Additionally, phenylthiazoles containing an *n*-alkyl chain lipophilic tail were found to be substrates for CYP450. This resulted in a very short half-life and high clearance rate ($t_{1/2}$ of **15a** <30 minutes, Fig. 1–8).[55] Based on the data presented in (Table 6), the toxicity hazards of all top hits were as predicted by the OSIRIS Property Explorer, and the two compounds have similar pharmacokinetic properties in many respects such as hepatic stability, but differ in their distribution and CNS activity. Compound **29** likely has a longer duration of action than linezolid and the first

Table 4 Binding energies (kcal mol^{-1}) and intermolecular bonds of compound **29** with the active sites of the cell wall proteins

Ligand	Dock score (kcal mol^{-1})	Affinity binding (kcal mol^{-1})	MM-GBSA (ΔG_{bind})	Interaction type	Interacting residues, distance (A^0), and energy (kcal mol^{-1})
PNAM	−11.48	−7.52	−8.53	Hydrogen bonding	SER403, 2.86, −1.2
				Hydrogen bonding	SER462, 2.69, −13.3
				Hydrogen bonding	ASN464, 3.35, −0.7
				Hydrogen bonding	THR600, 2.91, −4.8
				Hydrogen bonding	SER598, 2.51, −0.6
				Hydrogen bonding	TYR446, 4.49, −0.8
29	−11.95	−7.39	−7.88	Hydrogen bonding	SER 462, 3.10, −1.3
				Hydrogen bonding	SER403, 3.05, −1.9
				Aromatic stacking	TYR446, 4.14, −0.8
				Hydrogen bonding	ASN464, 4.35, −1.4
				Hydrophobic	Met641, Gln613, Gln637, 3.85, −2.3

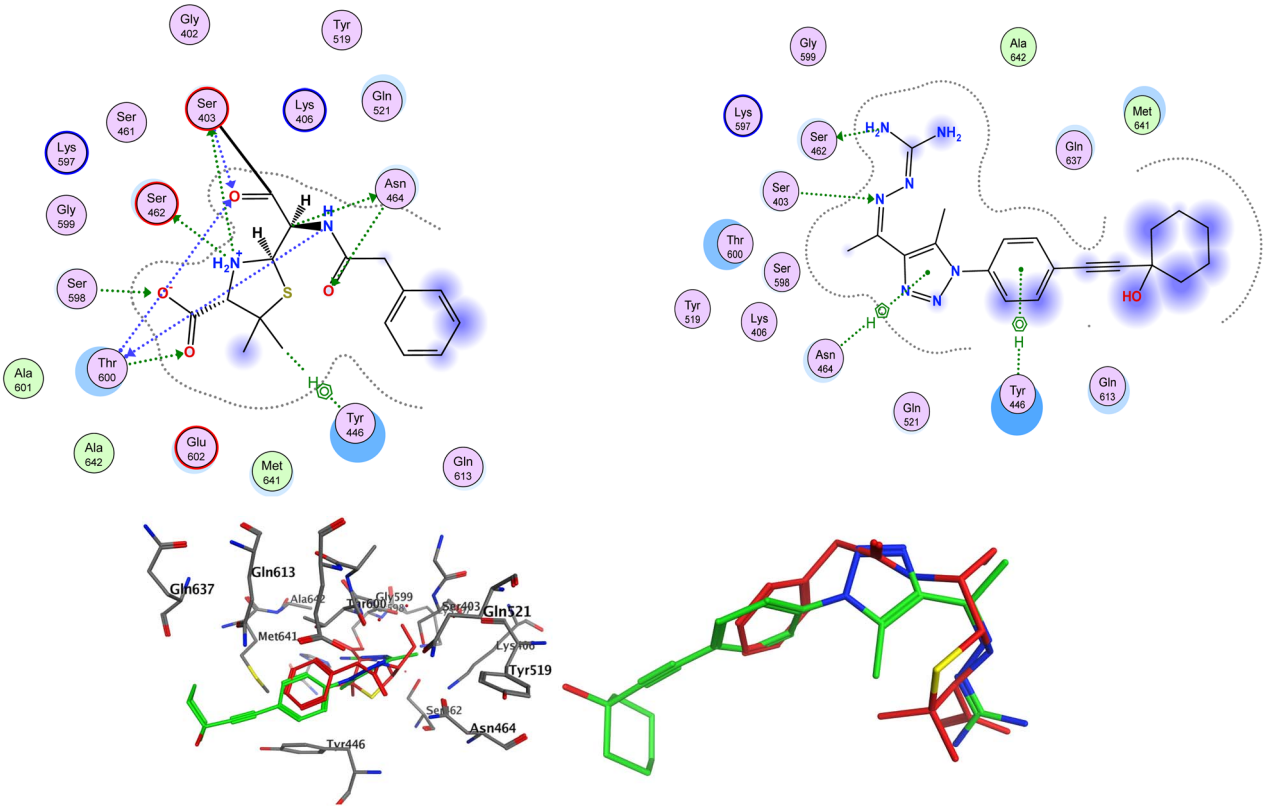

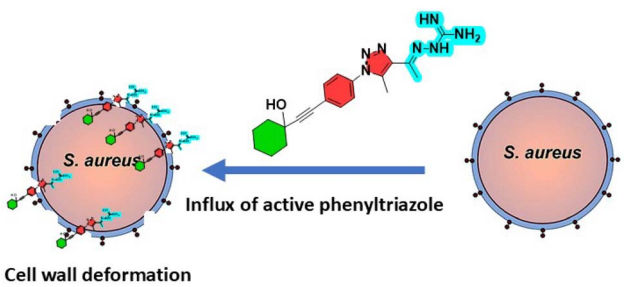

Fig. 8 Sketched diagram showing the mode of action of the novel scaffold.

Table 5 Prediction of the binding data and inhibition constants (Ki (nM)) of selected compounds against *S. aureus* penicillin-binding protein 2a

Compound	ΔG of binding (kcal mol^{-1})	Inhibition constant (Ki, nM)	Log *P*
20	−5.68	679.07	4.1
23	−6.60	143.01	4.9
29	−7.39	37.80	4.2
30	−7.21	51.21	5.1
31	−7.11	60.60	3.5
PNAM	−7.89	16.20	−0.86

Table 6 Predicted druglikeness and toxicity profiles of the top hits using OSIRIS property explorer

Parameter	**Compound 29**	Linezolid
Pharmacokinetic properties		
Hepatic stability	>50% at 60 minutes	>50% at 60 minutes
Microsomal half-life (tissue)	≤30 minutes	≤30 minutes
Renal clearance	<0.10 mL min^{-1} kg^{-1}	—
Plasma half-life	>12 hours	Between 1 and 6 hours
Oral bioavailability	>0.5 F	<0.5 F
Caco-2 permeability	Permeates Caco-2	Permeates Caco-2
BBB permeability	Permeates BBB	No
Microsomal intrinsic clearance	≥12 μL min^{-1} mg^{-1}	<12 μL min^{-1} mg^{-1}
Plasma protein binding	Plasma protein binder	Weak/non plasma protein binder
Microsomal half-life (sub-cellular)	>30 minutes	>30 minutes
CNS activity	Exhibits CNS activity	Exhibits CNS activity
Molecular properties		
Molecular weight	379	337
Log *P*	1.48	0.52
Solubility in water	−4.64 (77.23 mg L^{-1})	−2.96 (1454.87 mg L^{-1})
TPSA	125.2	71.1
Mutagenicity		
Tumorgenicity		
Irritating effects		
Reproductive effects		
Druglikeness	−7.45	−4.08
Drug score	0.35	0.45

generation of alkylphenylthiazole ($t_{1/2}$ = 4.4 h) due to its longer plasma half-life and higher plasma protein binding, while linezolid has better solubility and a slightly better druglikeness and drug score (Table 6). These parameters may lead to further modifications to optimize compound **29** as a potential therapeutic agent.

2.6. Conclusion

This study successfully showed the potential of phenyltriazole derivatives as effective anti-MRSA agents. Using rational design and scaffold hopping, a series of phenyltriazole compounds were synthesized and evaluated against methicillin-resistant *Staphylococcus aureus* (MRSA). The introduction of the 1,2,3-triazole ring, replacing the conventional thiazole core, was a strategic move aimed at enhancing the antimicrobial properties while improving the physicochemical properties of these molecules. Among the synthesized derivatives, compound **29** exhibited the most promising activity, with an MIC value comparable to or better than standard antibiotics such as vancomycin. Its rapid bactericidal action and significant disruption of MRSA biofilms make it a suitable candidate for the treatment of MRSA infections. The compound also showed a favorable selectivity index, highlighting its safety profile for therapeutic use. Molecular docking studies further supported the proposed mechanism of action and suggested a strong binding affinity to penicillin-binding protein 2a (PBP2a), which is crucial for cell wall biosynthesis in MRSA. This study not only highlights the importance of scaffold modifications but also provides valuable insights into the structure–activity relationship (SAR) of phenyltriazole compounds. The observed correlation between a terminal branched chain structure and antimicrobial efficacy highlights the critical role of molecular design in the development of effective antimicrobial agents. Future research should focus on optimizing the pharmacokinetic properties of these derivatives and exploring their efficacy *in vivo*. Additionally, expanding the scope to other resistant bacterial strains could further validate the potential of phenyltriazole scaffolds as broad-spectrum antibacterial agents. The

promising results of compound **29**, including its minimal cytotoxicity, potent anti-biofilm activity, and favorable pharmacokinetics, suggest that it could serve as a lead compound for the development of new antibiotics targeting resistant pathogens.

3. Experimental

3.1. Chemistry

The chemicals used in the synthetic protocols were purchased from Sigma-Aldrich Corp., USA. The melting points of the target compounds were uncorrected and recorded using a Stuart Scientific Co. Ltd apparatus. The IR analysis was done by a Jasco FT/IR 460 Plus spectrophotometer utilizing a KBr disc unit. The ^{1}H (400 MHz) and ^{13}C (100 MHz) NMR spectra were measured on a BRUKER AV 850 MHz spectrometer in DMSO-d_6 solvent using tetramethyl silane (TMS) as an internal standard. All compound purities were analyzed by HPLC-mass spectrometry on an Agilent 1100/ZQ MSD including a C18 column and diode array UV detector using a suitable mobile phase. In addition, elemental analysis data were recorded on an RCMP unit, Al-Azhar University, Cairo, Egypt. TLC on precoated Merck sheets was utilized for following reactions and separations.

3.1.1 General synthetic procedures for 1-azido-4-bromobenzene 2. Compound (**2**) was synthesized by dissolving 4-bromoaniline in H_2O : HCl (1 : 1) and stirred at 0–5 °C for 30 min. The aqueous $NaNO_2$ was added dropwise to form diazotize amine hydrochloride. After that the solution was treated with aqueous NaN_3 and further stirred for 1 h at room temperature. Finally, the reaction mixture was extracted with ethyl acetate, dried over anhydrous sodium sulphate and concentrated *in vacuo* to afford compound (**2**) in quantitative yield.[56]

3.1.2 Synthesis of 1-(1-(4-bromophenyl)-5-methyl-1*H*-1,2,3-triazol-4-yl)ethan-1-one 4. To a solution of sodium ethoxide (971 mg, 14.2 mmol) in anhydrous ethanol (20 mL) was added acetylacetone (**3**, 1.46 mL, 14.2 mmol) in an ice-bath for 30 min. Then, to this solution 1-azido-4-bromobenzene (**2**, 2 g, 7.14 mmol) in anhydrous ethanol (3 mL) was added dropwise. The mixture was stirred at room temperature for 24 h. The resulting suspension was filtered, and the solid product was washed with H_2O and ethanol to give **4** as light-yellow crystals; yield: 1.92 g, 96%; mp 118–120 °C.

3.1.3 1-(5-Methyl-1-(4-(alkyl or aryl-1-yn-1-yl)phenyl)-1*H*-1,2,3-triazol-4-yl)ethan-1-one 5–16. General procedure: To dry DME (25 mL) in a sealed tube, compound **4** (1 equiv.), appropriate alkynes (2 equiv.), triethylamine (3 mL), and potassium carbonate (2 equiv.) were added. After the reaction mixture was purged with dry nitrogen gas for 10 min, dichloro bis(triphenyl phosphine) palladium(II) (5% mole) and copper(I) iodide (7.5% mole) were added. The sealed tube was then placed in an oil bath and stirred at 110 °C for 24 h. After cooling to room temperature, the reaction mixture was extracted 3 times by ethyl acetate (20 mL). The combined organic layer was dried over $MgSO_4$ then concentrated under reduced pressure. The crude materials were purified *via* silica gel flash column chromatography using hexane-ethyl acetate (9 : 1). Yields, physical properties, and spectral data of isolated purified products are listed below.

3.1.4 1-(5-Methyl-1-(4-((trimethylsilyl)ethynyl)phenyl)-1*H*-1,2,3-triazol-4-yl)ethan-1-one 17, 18

*3.1.4.1 General procedures for compounds **17** and **18**.* To dry DME (5 mL) in a 25 mL sealed tube compound **4** (1 equiv.), ethynyltrimethylsilane (2 equiv.), and triethylamine (2 mL) were added. After the reaction mixture was purged with dry nitrogen gas for 20 min, dichlorobis(triphenylphosphine)palladium(II) (5% mol) and copper(I) iodide (7.5% mol) were added. The sealed tube was then placed in an oil bath and stirred at 50 °C for 2 h. After cooling down to room temperature, the reaction mixture was passed through Celite, followed by chloroform (2 × 50 mL). The organic materials were then concentrated under reduced pressure. The crude materials were purified and washed by silica gel flash column chromatography using hexane-ethyl acetate (9 : 1) to afford the intermediate compound 1-(5-methyl-1-(4-((trimethylsilyl)ethynyl)phenyl)-1*H*-1,2,3-triazol-4-yl)ethan-1-one.

3.1.4.2 1-(1-(4-Ethynylphenyl)-5-methyl-1H-1,2,3-triazol-4-yl) ethan-1-one. To dry methanol (10 mL) in a 25 mL round flask, the intermediate compound 1-(5-methyl-1-(4-((trimethylsilyl) ethynyl)phenyl)-1*H*-1,2,3-triazol-4-yl)ethan-1-one (1 equiv.) and anhydrous potassium carbonate (0.1% mol) were added. The reaction mixture was stirred at room temperature for 1 h until an off-white precipitate formed, and then concentrated under reduced pressure. The reaction was then quenched with very diluted hydrochloric acid and extracted with diethyl ether and then dried over anhydrous $MgSO_4$. The solvent was evaporated under reduced pressure and the product was used in the next step without purification.

*3.1.4.3 Compounds **17** and **18**.* Compounds **17** and **18** were prepared by the typical Sonogashira cross-coupling as mentioned above. Yields, physical properties, and spectral data of isolated purified products are listed below.

3.1.5 1-(5-Methyl-1-(4-(pent-1-yn-1-yl)phenyl)-1*H*-1,2,3-triazol-4-yl)ethan-1-one 5. Yellow oil (235 mg, 82%), ^{1}H NMR (DMSO-d_6); δ 8.10 (d, J = 8.1 Hz, 2H), 7.50 (d, J = 8.1 Hz, 2H), 2.67 (s, 3H), 2.46 (t, J = 7.8 Hz, 2H), 2.25 (s, 3H), 1.62–1.55 (m, 2H), 1.03 (t, J = 7.5 Hz, 3H); ^{13}C NMR (DMSO-d_6); δ 193.09, 148.38, 137.09, 132.04, 126.85, 124.03, 117.59, 92.34, 81.16, 25.31, 22.14, 21.15, 17.47, 13.86; ESI-MS (m/z); 267.33 (M^+, 99.91%).

3.1.6 1-(5-Methyl-1-(4-(4-methylpent-1-yn-1-yl)phenyl)-1*H*-1,2,3-triazol-4-yl)ethan-1-one 6. Light brown oil (240 mg, 79%): ^{1}H NMR (DMSO-d_6); δ 8.10 (d, J = 8.0 Hz, 2H), 7.50 (d, J = 8.0 Hz, 2H), 2.64 (s, 3H), 2.38 (d, J = 7.9 Hz, 2H), 2.23 (s, 3H), 1.92–1.85 (m, 1H), 1.04 (d, J = 8.1 Hz, 6H); ^{13}C NMR (DMSO-d_6); δ 200.65, 139.30, 137.19, 132.11, 129.39, 127.46, 125.16, 117.75, 91.98, 81.75, 29.89, 28.27, 28.08, 25.24, 22.27; MS (m/z); 281.36 (M^+, 62.41%).

3.1.7 1-(1-(4-(Hex-1-yn-1-yl)phenyl)-5-methyl-1*H*-1,2,3-triazol-4-yl)ethan-1-one 7. Brown oil (203 mg, 71%): ^{1}H NMR (DMSO-d_6); δ 8.09 (d, J = 8.1 Hz, 2H), 7.49 (d, J = 8.1 Hz, 2H), 2.64 (s, 3H), 2.45 (t, J = 7.9 Hz, 2H), 2.24 (s, 3H), 1.59–1.32 (m, 4H), 0.93 (t, J = 7.9 Hz, 3H); ^{13}C NMR (DMSO-d_6); δ 192.63, 152.43, 138.20, 137.09, 135.70, 132.05, 132.02, 126.84, 117.59,

92.52, 81.97, 31.04, 28.35, 25.31, 22.13, 17.48, 14.36; MS (*m*/*z*); 281.35 (M^+, 69.41%).

3.1.8 1-(5-Methyl-1-(4-(oct-1-yn-1-yl)phenyl)-1*H*-1,2,3-triazol-4-yl)ethan-1-one 8. Brown oil (235 mg, 71%): ^{1}H NMR (DMSO-d_6); δ 8.09 (d, J = 8.1 Hz, 2H), 7.48 (d, J = 8.1 Hz, 2H), 2.64 (s, 3H), 2.47 (t, J = 7.2 Hz, 2H), 2.23 (s, 3H), 1.60–1.29 (m, 8H), 0.91 (t, J = 6.1 Hz, 3H); ^{13}C NMR (DMSO-d_6); δ 191.81, 138.21, 137.09, 135.80, 132.03, 126.85, 124.04, 117.59, 92.52, 81.01, 31.23, 28.60, 25.32, 22.50, 19.20, 17.45, 14.40; MS (*m*/*z*); 309.18 (M^+, 77.41%).

3.1.9 1-(1-(4-(3,3-Dimethylbut-1-yn-1-yl)phenyl)-5-methyl-1*H*-1,2,3-triazol-4-yl)ethan-1-one 9. Yellow oil (250 mg, 82%); ^{1}H NMR (DMSO-d_6); δ 8.10 (d, J = 8.1 Hz, 2H), 7.46 (d, J = 8.1 Hz, 2H), 2.64 (s, 3H), 2.23 (s, 3H), 1.32 (s, 9H); ^{13}C NMR (DMSO-d_6); δ 198.58, 138.14, 137.09, 135.04, 132.04, 126.76, 123.90, 117.56, 100.23, 79.41, 31.22, 28.14, 25.31, 17.47; MS (*m*/*z*); 281.36 (M^+, 92.31%).

3.1.10 1-(1-(4-(Cyclopropylethynyl)phenyl)-5-methyl-1*H*-1,2,3-triazol-4-yl)ethan-1-one 10. Yellow oil (244 mg, 86%); ^{1}H NMR (DMSO-d_6); δ 8.08 (d, J = 8.2 Hz, 2H), 7.46 (d, J = 8.2 Hz, 2H), 2.64 (s, 3H), 2.23 (s, 3H), 1.61–1.55 (m, 1H), 0.93–0.90 (m, 2H), 0.78–0.75 (m, 2H); ^{13}C NMR (DMSO-d_6); δ 197.19, 152.76, 144.96, 140.02, 133.21, 132.04, 130.02, 118.13, 117.95, 116.52, 95.21, 81.56, 27.38, 24.45, 18.26, 10.05, 1.02; MS (*m*/*z*); 265.32 (M^+, 78.61%).

3.1.11 1-(1-(4-(Cyclopentylethynyl)phenyl)-5-methyl-1*H*-1,2,3-triazol-4-yl)ethan-1-one 11. Brown oil (230 mg, 73%); ^{1}H NMR (DMSO-d_6); δ 7.70 (d, J = 8.1 Hz, 2H), 7.49 (d, J = 8.1 Hz, 2H), 2.90–2.86 (m, 1H), 2.70 (s, 3H), 2.60 (s, 3H), 2.00–1.55 (m, 8H); ^{13}C NMR (DMSO-d_6); δ 200.64, 139.29, 132.21, 131.53, 129.39, 127.41, 125.19, 117.78, 97.07, 80.36, 33.91, 30.60, 29.87, 25.11, 24.94; MS (*m*/*z*); 293.37 (M^+, 62.61%).

3.1.12 1-(1-(4-(Cyclohexylethynyl)phenyl)-5-methyl-1*H*-1,2,3-triazol-4-yl)ethan-1-one 12. Light brown oil (250 mg, 76%); ^{1}H NMR (DMSO-d_6); δ 8.08 (d, J = 8.2 Hz, 2H), 7.48 (d, J = 8.2 Hz, 2H), 2.64 (s, 3H), 2.24 (s, 3H), 1.87–1.31 (m, 11H); ^{13}C NMR (DMSO-d_6); δ 197.11, 155.06, 153.56, 148.12, 138.71, 137.44, 135.62, 132.41, 126.95, 124.72, 96.34, 81.36, 33.12, 29.93, 25.05, 24.97, 17.15, 14.12; MS (*m*/*z*); 307.43 (M^+, 69.61%).

3.1.13 1-(1-(4-(4-Hydroxyhex-1-yn-1-yl)phenyl)-5-methyl-1*H*-1,2,3-triazol-4-yl)ethan-1-one 13. Yellow oil (265 mg, 83%); ^{1}H NMR (DMSO-d_6); δ 8.13 (d, J = 8.2 Hz, 2H), 7.54 (d, J = 8.2 Hz, 2H), 5.72 (brs, 1H), 3.66–3.61 (m, 1H), 2.65 (s, 3H), 2.23 (s, 3H), 1.99–1.97 (m, 2H) 1.51 (d, J = 7.9 Hz, 2H), 1.18 (t, J = 8.1 Hz, 3H); ^{13}C NMR (DMSO-d_6); δ 200.29, 155.75, 148.32, 137.12, 132.21, 126.90, 117.71, 99.52, 86.19, 59.29, 32.07, 29.15, 25.32, 17.46, 16.19; MS (*m*/*z*); 297.36 (M^+, 88.31%).

3.1.14 1-(1-(4-(3-Hydroxy-3-methylbut-1-yn-1-yl)phenyl)-5-methyl-1*H*-1,2,3-triazol-4-yl)ethan-1-one 14. Yellow oil (245 mg, 81%); ^{1}H NMR (DMSO-d_6); δ 8.13 (d, J = 8.4 Hz, 2H), 7.54 (d, J = 8.4 Hz, 2H), 5.44 (brs, 1H), 2.65 (s, 3H), 2.23 (s, 3H), 1.51 (s, 6H); ^{13}C NMR (DMSO-d_6); δ 204.01, 153.41, 144.96, 139.98, 133.65, 132.94, 130.04, 118.73, 117.85, 116.82, 95.76, 81.63, 64.36, 33.88, 26.96 18.65; MS (*m*/*z*); 283.33 (M^+, 72.45%).

3.1.15 1-(1-(4-((1-Hydroxycyclohexyl)ethynyl)phenyl)-5-methyl-1*H*-1,2,3-triazol-4-yl)ethan-1-one 15. Yellow oil (270 mg, 78%); ^{1}H NMR (DMSO-d_6); δ 8.12 (d, J = 8.2 Hz, 2H), 7.81 (d, J = 8.2 Hz, 2H), 6.23 (brs, 1H), 2.65 (s, 3H), 2.26 (s, 3H), 2.18–1.51 (m, 10H); ^{13}C NMR (DMSO-d_6); δ 198.18, 137.20, 136.12, 132.23, 131.93, 126.93, 117.66, 93.05, 87.29, 58.38, 37.26, 29.23, 25.74, 25.19, 17.68, 16.25; MS (*m*/*z*); 323.33 (M^+, 61.61%).

3.1.16 1-(5-Methyl-1-(4-(phenylethynyl)phenyl)-1*H*-1,2,3-triazol-4-yl)ethan-1-one 16. Brown oil (210 mg, 65%); ^{1}H NMR (DMSO-d_6); δ 8.19 (d, J = 8.2 Hz, 2H), 8.16 (d, J = 8.2 Hz, 2H), 7.85–7.44 (m, 5H), 2.67 (s, 3H), 2.25 (s, 3H); ^{13}C NMR (DMSO-d_6); δ 197.72, 139.02, 137.13, 135.85, 132.24, 131.88, 129.36, 127.01, 122.72, 117.77, 117.74, 91.01, 89.84, 25.34, 17.50; MS (*m*/*z*); 301.35 (M^+, 48.51%).

3.2 Synthesis of 1-(5-methyl-1-(4-substituted aryl)-1*H*-1,2,3-triazol-4-yl)ethan-1-one (17–18)

3.2.1 General procedure

*3.2.1.1 Synthesis of 1-(5-methyl-1-(4-((trimethylsilyl)ethynyl) phenyl)-1H-1,2,3-triazol-4-yl)ethan-1-one **4a**.* To dry DME (25 mL) in a sealed tube, compound **4** (1 mmol, 1 equiv.), appropriate alkynes (2 mmol, 2 equiv.), triethylamine (3 mL), and potassium carbonate (2 mmol, 2 equiv.) were added. After the reaction mixture was purged with dry nitrogen gas for 10 min, dichloro bis(triphenyl phosphine) palladium(II) (5% mole) and copper(I) iodide (7.5% mole) were added. The sealed tube was then placed in an oil bath and stirred at 110 °C for 24 h. After cooling to room temperature, the reaction mixture was extracted 3 times by ethyl acetate (20 mL). The organic materials were then concentrated under reduced pressure. The crude materials were purified by silica gel flash column chromatography using hexane-ethyl acetate (9 : 1). The yield was 500 mg (94%).

*3.2.1.2 Deprotection step to synthesis 1-(1-(4-ethynylphenyl)-5-methyl-1H-1,2,3-triazol-4-yl) ethan-1-one **4b**.* To dry methanol (10 mL) in a 25 mL round flask compound **4a** (300 mg, 1.07 mmol) and anhydrous potassium carbonate (70 mg, 0.5 mmol) were added. The reaction mixture was stirred at room temperature for 1 h until an off-white precipitate formed, and then concentrated under reduced pressure. It was then quenched with very dilute hydrochloric acid and extracted with diethyl ether, and then dried over anhydrous $MgSO_4$. The solvent was evaporated under reduced pressure. The yield was 200 mg (88%).

3.2.2 1-(5-Methyl-1-(4-(*p*-tolylethynyl)phenyl)-1*H*-1,2,3-triazol-4-yl)ethan-1-one 17. To dry DME (10 mL) in a 25 mL sealed tube compound **4b** (200 mg, 0.88 mmol), 4-bromotoluene (151 mg, 0.88 mmol), and triethylamine (2 mL) were added. After the reaction mixture was purged with dry nitrogen gas for 10 min, dichlorobis(triphenylphosphine)palladium(II) (31 mg, 0.44 mmol) and copper(I) iodide (13 mg, 0.66 mmol) were added. The sealed tube was then placed in an oil bath and stirred at 120 °C for 24 h. After cooling down to room temperature, the reaction mixture was passed through Celite, followed by chloroform (2 × 50 mL). The organic materials were then concentrated under reduced pressure. The crude materials were purified by silica gel flash column chromatography using hexane-ethyl acetate (7 : 3). The yield, physical properties and spectral data of the isolated purified product are listed below.

Brown oil (190 mg, 67%); ^{1}H NMR (DMSO-d_6); δ 8.19 (d, J = 8.2 Hz, 2H), 8.16 (d, J = 8.2 Hz, 2H), 7.85–7.44 (m, 4H), 2.67 (s,

3H), 2.25 (s, 3H), 2.16 (s, 3H); ^{13}C NMR (DMSO-d_6); δ 199.03, 155.79, 152.25, 148.44, 139.26, 137.13, 129.36, 127.01, 122.72, 117.77, 117.74, 91.01, 89.79, 25.34, 23.61, 17.50; MS (*m*/*z*); 315.38 (M^+, 77.51%).

3.2.3 1-(5-Methyl-1-(4-(thiophen-3-ylethynyl)phenyl)-1*H*-1,2,3-triazol-4-yl)ethan-1-one 18. Brown oil (200 mg, 73%); ^{1}H NMR (DMSO-d_6); δ 8.30 (d, J = 8.2 Hz, 1H), 7.92 (d, J = 8.2 Hz, 2H), 7.78 (s, 1H), 7.73 (d, J = 8.2 Hz, 2H), 7.03 (d, J = 8.2 Hz, 1H), 2.60 (s, 3H), 2.32 (s, 3H); ^{13}C NMR (DMSO-d_6); δ 191.07, 158.72, 142.58, 136.89, 132.47, 131.38, 129.30, 127.79, 127.52, 126.43, 125.49, 98.00, 82.92, 30.89, 18.65; MS (*m*/*z*); 307.37 (M^+, 74.51%).

3.2.4 2-(1-(5-Methyl-1-(4-(alkynyl)phenyl)-1*H*-1,2,3-triazol-4-yl)ethylidene)hydrazine-1-carboximidamide 19–32. General procedure: phenyltriazol-acetyl derivatives **5–18** (1 equiv.) were dissolved in absolute ethanol (10 mL), and concentrated hydrochloric acid (0.2 mL) and aminoguanidine hydrochloride (2 equiv.) were added. The reaction mixture was heated under reflux for 4 h. The solvent was concentrated under reduced pressure, then poured into crushed ice and neutralized with potassium carbonate to pH 9–10, and the formed precipitated solid was collected by filtration and washed with copious amounts of water. Crystallization was from DCM to afford the desired products as solids. The yield, physical properties and spectral data of the isolated purified product are listed below.

3.2.5 2-(1-(5-Methyl-1-(4-(pent-1-yn-1-yl)phenyl)-1*H*-1,2,3-triazol-4-yl)ethylidene)hydrazine-1-carboximidamide 19. Off-white solid (95 mg, 78%); mp. 205–207 °C; ^{1}H NMR (DMSO-d_6); δ 8.10 (d, J = 8.4 Hz, 2H), 7.50 (d, J = 8.4 Hz, 2H), 5.72 (brs, 2H), 5.52 (brs, 2H), 2.67 (s, 3H), 2.64 (t, J = 7.1 Hz, 2H), 2.25 (s, 3H), 1.64 (m, 2H), 1.05 (t, J = 7.6 Hz, 3H); ^{13}C NMR (DMSO-d_6); δ 160.31, 148.33, 138.22, 137.09, 135.73, 132.04, 126.85, 124.03, 117.59, 92.34, 81.16, 25.31, 22.14, 21.15, 17.47, 13.86; MS *m*/*z* (%): 323 (M^+, 39.55); purity *via* HPLC = 98.07%; anal. calc. for: $C_{17}H_{21}N_7$ (323): C, 63.14; H, 6.55; N, 30.32%; found: C, 63.09; H, 6.48; N, 30.49%.

3.2.6 2-(1-(5-Methyl-1-(4-(4-methylpent-1-yn-1-yl)phenyl)-1*H*-1,2,3-triazol-4-yl)ethylidene)hydrazine-1-carboximidamide 20. Yellowish-white solid (90 mg, 71%); mp 195–197 °C, ^{1}H NMR (DMSO-d_6); δ 8.10 (d, J = 8.4 Hz, 2H), 7.50 (d, J = 8.6 Hz, 2H), 5.71 (brs, 2H), 5.51 (brs, 2H), 2.64 (s, 3H), 2.38 (d, J = 7.6 Hz, 2H), 2.23 (s, 3H), 1.92–1.85 (m, 1H), 1.04 (d, J = 7.6 Hz, 6H); ^{13}C NMR (DMSO-d_6); δ 160.33, 155.68, 138.22, 137.10, 135.05, 132.86, 124.04, 117.55, 91.36, 81.90, 28.26, 28.11, 25.32, 22.31, 17.47; MS *m*/*z* (%): 337 (M^+, 55.75); purity *via* HPLC = 99.33%; anal. calc. for: $C_{18}H_{23}N_7$ (337): C, 64.07; H, 6.87; N, 29.06%; found: C, 64.13; H, 6.92; N, 29.10%.

3.2.7 2-(1-(1-(4-(Hex-1-yn-1-yl)phenyl)-5-methyl-1*H*-1,2,3-triazol-4-yl)ethylidene)hydrazine-1-carboximidamide 21. White solid (100 mg, 79%); mp 199–201 °C, ^{1}H NMR (DMSO-d_6); δ 8.09 (d, J = 8.4 Hz, 2H), 7.49 (d, J = 8.6 Hz, 2H), 5.74 (brs, 2H), 5.55 (brs, 2H), 2.64 (s, 3H), 2.47 (t, J = 7.1 Hz, 2H), 2.24 (s, 3H), 1.61–130 (m, 4H), 0.93 (t, J = 7.2 Hz, 3H); ^{13}C NMR (DMSO-d_6); δ 160.29, 155.68, 138.20, 137.09, 135.70, 132.05, 126.84, 124.05, 117.59, 92.52, 80.97, 31.04, 28.35, 25.31, 22.13, 17.48, 14.36; MS *m*/*z* (%): 337 (M^+, 59.75); purity *via* HPLC = 99.33%; anal. calc. for: $C_{18}H_{23}N_7$ (337): C, 64.07; H, 6.87; N, 29.06%; found: C, 64.13; H, 6.92; N, 29.10%.

3.2.8 2-(1-(1-(4-(Oct-1-yn-1-yl)phenyl)-5-methyl-1*H*-1,2,3-triazol-4-yl)ethylidene)hydrazine-1-carboximidamide 22. Light brown solid (95 mg, 77%): mp. 206–208 °C; ^{1}H NMR (DMSO-d_6); δ 8.09 (d, J = 8.4 Hz, 2H), 7.48 (d, J = 8.4 Hz, 2H), 5.72 (brs, 2H), 5.52 (brs, 2H), 2.64 (s, 3H), 2.47 (t, J = 7.2 Hz, 2H), 2.23 (s, 3H), 1.60–130 (m, 8H), 0.91 (t, J = 7.6 Hz, 3H); ^{13}C NMR (DMSO-d_6); δ 160.35, 155.67, 138.21, 137.73, 135.73, 132.03, 126.85, 127.04, 117.53, 92.52, 81.01, 31.23, 28.60, 25.23, 22.50, 19.20, 17.46, 14.40; MS *m*/*z* (%): 365 (M^+, 66.15); purity *via* HPLC = 98.61%; anal. calc. for: $C_{20}H_{27}N_7$ (365): C, 65.73; H, 7.45; N, 26.83%; found: C, 65.81; H, 7.62; N, 26.61%.

3.2.9 2-(1-(1-(4-(3,3-Dimethylbut-1-yn-1-yl)phenyl)-5-methyl-1*H*-1,2,3-triazol-4-yl)ethylidene) hydrazine-1-carboximidamide 23. Beige solid (105 mg, 83%); mp 201–203 °C, ^{1}H NMR (DMSO-d_6); δ 8.10 (d, J = 8.4 Hz, 2H), 7.46 (d, J = 8.4 Hz, 2H), 5.72 (brs, 2H), 5.52 (brs, 2H), 2.64 (s, 3H), 2.23 (s, 3H), 1.32 (s, 9H); ^{13}C NMR (DMSO-d_6); δ 160.36, 155.67, 138.14, 137.09, 135.80, 132.04, 126.76, 123.90, 117.49, 100.27, 79.41, 31.22, 28.14, 25.31, 17.47; MS *m*/*z* (%): 337 (M^+, 88.43); purity *via* HPLC = 99.74%; anal. calc. for: $C_{18}H_{23}N_5$ (337): C, 64.07; H, 6.87; N, 29.06%; found: C, 64.13; H, 6.92; N, 29.10%.

3.2.10 2-(1-(1-(4-(Cyclopropylethynyl)phenyl)-5-methyl-1*H*-1,2,3-triazol-4-yl)ethylidene)hydrazine-1-carboximidamide 24. Yellow solid (97 mg, 82%); mp 205–207 °C, ^{1}H NMR (DMSO-d_6); δ 8.08 (d, J = 8.4 Hz, 2H), 7.47 (d, J = 8.4 Hz, 2H), 5.72 (brs, 2H), 5.53 (brs, 2H), 2.64 (s, 3H), 2.23 (s, 3H), 1.61–1.55 (m, 1H), 0.94–0.89 (m, 2H), 0.79–0.75 (m, 2H); ^{13}C NMR (DMSO-d_6); δ 159.50, 154.52, 137.27, 136.23, 134.86, 131.23, 125.96, 123.10, 116.67, 94.81, 75.23, 24.47, 16.62, 8.11, 0.50; MS *m*/*z* (%): 321 (M^+, 87.13); purity *via* HPLC = 98.23%; anal. calc. for $C_{17}H_{19}N_7$ (321); anal. calc. for: $C_{17}H_{19}N_7$ (321): C, 63.53; H, 5.96; N, 30.51%; found: C, 63.63; H, 6.02; N, 30.10%.

3.2.11 2-(1-(1-(4-(Cyclopentylethynyl)phenyl)-5-methyl-1*H*-1,2,3-triazol-4-yl)ethylidene)hydrazine-1-carboximidamide 25. Brown solid (90 mg, 69%); mp 210–212 °C, ^{1}H NMR (DMSO-d_6); δ 8.09 (d, J = 8.6 Hz, 2H), 7.48 (d, J = 8.6 Hz, 2H), 5.74 (brs, 2H), 5.56 (brs, 2H), 2.93–2.85 (m, 1H), 2.64 (s, 3H), 2.23 (s, 3H), 2.02–1.57 (m, 8H); ^{13}C NMR (DMSO-d_6); δ 160.33, 155.67, 138.12, 137.08, 135.69, 132.02, 126.80, 124.07, 117.56, 96.45, 80.47, 33.95, 30.58, 25.31, 25.10, 17.47; MS *m*/*z* (%): 349 (M^+, 55.63); purity *via* HPLC = 96.24%; anal. calc. for: $C_{19}H_{23}N_7$ (349): C, 65.31; H, 6.63; N, 28.06%; found: C, 65.43; H, 6.72; N, 27.90%.

3.2.12 2-(1-(1-(4-(Cyclohexylethynyl)phenyl)-5-methyl-1*H*-1,2,3-triazol-4-yl)ethylidene)hydrazine-1-carboximidamide 26. Brown solid (98 mg, 72%); mp 216–218 °C. ^{1}H NMR (DMSO-d_6); δ 8.08 (d, J = 8.2 Hz, 2H), 7.48 (d, J = 8.2 Hz, 2H), 5.77 (brs, 2H), 5.60 (brs, 2H), 2.64 (s, 3H), 2.24 (s, 3H), 1.87–1.28 (m, 11H); ^{13}C NMR (DMSO-d_6); δ 160.27, 155.68, 138.16, 137.09, 135.67, 132.07, 126.81, 124.02, 117.57, 96.20, 80.97, 32.66, 29.36, 25.83, 25.29, 24.69, 17.49; MS *m*/*z* (%): 363 (M^+, 59.67); purity *via* HPLC = 98.97%; anal. calc. for: $C_{20}H_{25}N_7$ (363): C, 66.09; H, 6.93; N, 26.98%; found: C, 66.21; H, 7.02; N, 26.87%.

3.2.13 2-(1-(1-(4-(4-Hydroxyhex-1-yn-1-yl)phenyl)-5-methyl-1*H*-1,2,3-triazol-4-yl)ethylidene) hydrazine-1-carboximidamide 27. Yellow solid (105 mg, 79%); mp 222–224 °C. ^{1}H NMR

(DMSO-d_6); δ 8.11 (d, J = 8.1 Hz, 2H), 7.53 (d, J = 8.1 Hz, 2H), 5.72 (brs, 1H), 5.52 (brs, 2H), 5.44 (brs, 2H), 3.66–3.61 (m, 1H), 2.65 (s, 3H), 2.23 (s, 3H), 1.99–1.97 (m, 2H) 1.51 (d, J = 7.9 Hz, 2H), 1.18 (t, J = 8.1 Hz, 3H); ^{13}C NMR (DMSO-d_6); δ 160.36, 155.73, 152.21, 148.32, 137.12, 135.88, 132.21, 126.90, 117.71, 98.62, 89.88, 59.29, 32.07, 29.15, 25.32, 17.46, 16.19; MS m/z (%): 353 (M^+, 75.63); purity *via* HPLC = 98.16%; anal. calc. for: $C_{18}H_{23}N_7O$ (353): C, 61.17; H, 6.56; N, 27.74%; found: C, 61.25; H, 6.62; N, 27.64%.

3.2.14 2-(1-(1-(4-(3-Hydroxy-3-methylbut-1-yn-1-yl)phenyl)-5-methyl-1*H*-1,2,3-triazol-4-yl)ethylidene) hydrazine-1-carboximidamide 28. Yellow solid (99 mg, 77%); mp 219–221 °C. ^{1}H NMR (DMSO-d_6); δ 8.13 (d, J = 8.6 Hz, 2H), 7.54 (d, J = 8.4 Hz, 2H), 5.72 (brs, 2H), 5.52 (brs, 2H), 5.45 (brs, 1H), 2.65 (s, 3H), 2.23 (s, 3H), 1.51 (s, 6H); ^{13}C NMR (DMSO-d_6); δ 160.36, 155.73, 148.32, 137.12, 135.88, 132.21, 126.90, 122.72, 117.71, 89.88, 70.29, 59.29, 29.15, 25.32, 17.46; MS m/z (%): 339 (M^+, 85.53); purity *via* HPLC = 99.21%; anal. calc. for: $C_{17}H_{21}N_7O$ (339): C, 60.16; H, 6.24; N, 28.89%; found: C, 60.26; H, 6.37; N, 28.77%.

3.2.15 2-(1-(1-(4-((1-Hydroxycyclohexyl)ethynyl)phenyl)-5-methyl-1*H*-1,2,3-triazol-4-yl)ethylidene) hydrazine-1-carboximidamide 29. Brown solid (110 mg, 77%); mp 223–224 °C. ^{1}H NMR (DMSO-d_6); δ 8.12 (d, J = 8.2 Hz, 2H), 7.81 (d, J = 8.2 Hz, 2H), 6.22 (brs, 1H), 6.02 (brs, 4H), 2.65 (s, 3H), 2.26 (s, 3H), 2.20–1.15 (m, 10H); ^{13}C NMR (DMSO-d_6); δ 159.81, 155.76, 152.52, 149.00, 137.20, 136.12, 132.23, 126.93, 117.66, 93.05, 87.29, 58.38, 37.26, 29.23, 25.19, 21.47, 17.68, 16.25; MS m/z (%): 379 (M^+, 79.67); purity *via* HPLC = 99.01%; anal. calc. for: $C_{20}H_{25}N_7O$ (379): C, 63.30; H, 6.64; N, 25.84%; found: C, 63.41; H, 6.72; N, 25.77%.

3.2.16 2-(1-(5-Methyl-1-(4-(phenylethynyl)phenyl)-1*H*-1,2,3-triazol-4-yl)ethylidene)hydrazine-1-carboximidamide 30. Light brown solid (95 mg, 80%); mp 258–260 °C. ^{1}H NMR (DMSO-d_6); δ 8.19 (d, J = 8.4 Hz, 2H), 8.16 (d, J = 8.4 Hz, 2H), 7.85–7.44 (m, 5H), 5.78 (brs, 2H), 5.62 (brs, 2H), 2.67 (s, 3H), 2.25 (s, 3H); ^{13}C NMR (DMSO-d_6); δ 160.33, 155.79, 139.02, 137.13, 135.85, 132.22, 131.88, 129.27, 127.01, 122.92, 117.77, 117.74, 91.01, 89.84, 25.34, 17.50; MS (m/z); 357.42 (M^+, 78.51%).; purity *via* HPLC = 98.97%; anal. calc. for: $C_{20}H_{19}N_7$ (357.42): C, 67.21; H, 5.36; N, 27.43%; found: C, 67.33; H, 5.49; N, 27.37%.

3.2.17 2-(1-(5-Methyl-1-(4-(*p*-tolylethynyl)phenyl)-1*H*-1,2,3-triazol-4-yl)ethylidene)hydrazine-1-carboximidamide 31. Brown solid (98 mg, 79%); mp 268–270 °C. ^{1}H NMR (DMSO-d_6); δ 8.19 (d, J = 8.4 Hz, 2H), 8.16 (d, J = 8.4 Hz, 2H), 7.85–7.44 (m, 4H), 5.79 (brs, 2H), 5.62 (brs, 2H), 2.67 (s, 3H), 2.25 (s, 3H), 2.16 (s, 3H); ^{13}C NMR (DMSO-d_6); δ 160.33, 155.79, 152.25, 148.44, 139.26, 137.13, 132.24, 131.88, 129.27, 127.01, 122.92, 117.77, 90.96, 89.79, 25.34, 23.61, 17.50; MS (m/z); 371.44 (M^+, 88.54%); purity *via* HPLC = 97.54%; anal. calc. for: $C_{21}H_{21}N_7$ (371.45): C, 67.90; H, 5.70; N, 26.40%; found: C, 67.99; H, 5.82; N, 26.27%.

3.2.18 2-(1-(5-Methyl-1-(4-(thiophen-3-ylethynyl)phenyl)-1*H*-1,2,3-triazol-4-yl)ethylidene) hydrazine-1-carboximidamide 32. Yellow solid (88 mg, 72%); ^{1}H NMR (DMSO-d_6); δ 7.94 (d, J = 8.2 Hz, 2H), 7.77 (d, J = 8.2 Hz, 2H), 7.62–7.17 (m, 3H), 5.79 (brs, 2H), 5.67 (brs, 2H), 2.60 (s, 3H), 2.33 (s, 3H); ^{13}C NMR (DMSO-d_6); δ 162.27, 160.19, 148.37, 143.15, 141.04, 136.74, 135.28, 132.28, 127.83, 127.08, 126.70, 122.29, 98.00, 82.92, 18.70, 16.56; MS (m/z); 363.44 (M^+, 78.31%); purity *via* HPLC = 97.11%; anal. calc. for: $C_{18}H_{17}N_7S$ (363.44): C, 59.49; H, 4.71; N, 26.98%; found: C, 59.54; H, 4.83; N, 26.77%.

3.3. Biological screening

3.3.1 Antibacterial assay. The minimum inhibitory concentrations (MICs) of the tested compounds and control drugs, linezolid, vancomycin and gentamicin (antibiotics), and fluconazole and 5-fluorocytosine (5-FC) (antifungal drugs) were determined using the broth microdilution method according to Clinical and Laboratory Standards Institute guidelines.[57] The assay was conducted at the Department of Comparative Pathobiology, College of Veterinary Medicine, Purdue University, West Lafayette, USA. The strains used are clinically relevant bacterial strains (methicillin-resistant *Staphylococcus aureus* (MRSA), *Escherichia coli, Clostridium difficile* and *Neisseria gonorrhea* strains) and fungal strains (*Candida albicans*). *S. aureus* and *E. coli* were grown aerobically overnight on tryptone-soy agar plates at 37 °C. *C. difficile* agar was supplemented with brain-heart infusion at 37 °C for 48 h. *N. gonorrhea* was grown on Brucella broth supplemented with yeast extract, neopeptone, hematin, pyridoxal and NAD for 24 h at 37 °C in the in presence of 5% CO_2. *C. albicans* was grown aerobically overnight on a yeast peptone-dextrose agar plate (YPD) at 35 °C. A bacterial solution equivalent to 0.5 McFarland standard was then prepared and diluted in cation-adjusted Mueller-Hinton broth (CAMHB) (for *S. aureus* and *E. coli*) to achieve a bacterial concentration of approximately 5×10^5 CFU mL^{-1}. *C. difficile* was diluted in broth supplemented with brain heart infusion and supplemented with yeast extract, hemin and vitamin K to achieve a bacterial concentration of approximately 5×10^5 CFU mL^{-1}. *N. gonorrhoea* was diluted in Brucella broth supplemented with yeast extract, neopeptone, hematin, pyridoxal and NAD to achieve a bacterial concentration of approximately 1×10^6 CFU mL^{-1}. *C. albicans* was diluted in Roswell Park Memorial Institute medium (RPMI 1640) with glutamine and without bicarbonate (GIBCO from Life Technologies, Green Island, NY, USA) which was buffered to pH 7.0 with 0.165 M of [3-(*N*-morpholino) propanesulfonic acid] (MOPS) (Dot Scientific Inc., Burton, MI, USA) to achieve a fungal concentration of about 1.5×10^3 CFU mL^{-1}. Compounds and control drugs were added to the first row of the 96-well plates and serially diluted with the corresponding media containing bacteria/fungi. Plates were then incubated aerobically at 37 °C for 18–20 hours (for *S. aureus* and *E. coli*). *C. albicans* was incubated aerobically at 37 °C for 24 hours. The minimal inhibitory concentration (MIC, μg mL^{-1}) referred to the lowest concentration of new compounds that was required to completely arrest the growth of microbes.[58] The minimal bactericidal concentration (MBC, μg mL^{-1}) referred to the lowest concentration of new compounds that was required to completely kill microbes.[59] All results are mean values from at least three experiments.

3.3.2 MTT cytotoxicity evaluation. The MTT assay was performed in VACSERA, Giza, Egypt to confirm the cell viability of the two treated normal cell lines. Aneuploid immortal

keratinocyte cells (HaCaT), and well-established normal fibroblast cell lines (WI38) as well as neuro-HiB5 cells originally derived from the embryonic (E16) Sprague-Dawley rat hippocampus were employed, using colorimetric activities of the yellow MTT (3-(4,5-dimethyl thiazol-2-yl)-2,5-diphenyltetrazolium bromide).[60,61] See detailed description in the ESI data.†

3.3.3 Antibiofilm screening. The biofilm inhibitory activities of selected potent analogs at the corresponding MICs for each compound were assessed against highly biofilm forming methicillin resistant *Staphylococcus aureus* (MRSA) (3.655), *Candida albicans* (4.025) and *Pseudomonas aeruginosa* (3.198). The biofilm assay was carried out at the Department of Microbiology, Faculty of Pharmacy, Al-Azhar University, Cairo. Briefly, the freshly obtained seed culture was inoculated at a ratio of 1 : 100 in a 96-well micro-titer plate of polypropylene material. The plate was covered and incubated at 37 °C for 24 h to culture the biofilms. Each experiment always had a negative control (culture media only) and positive control (culture media with inoculation 1%). All experiments were conducted in replicates of three unless otherwise mentioned.[62] Crystal violet assay was performed to assess the biofilm inhibiting activity of the chemical compounds. For biofilm inhibition assay the medium and planktonic cells were discarded after 24 h of static growth at 37 °C. Each well was rinsed thrice unless and until complete removal of all media and planktonic cells. Adhered cells were stained with 125 μL of crystal violet (0.1%) for 30 min at room temperature. Then the crystal violet (CV) was washed out while using d.H_2O. The CV bound to biofilm was re-solubilized in 30% acetic acid and its absorbance was measured at 550 nm.[63–65] The change in the biofilm was calculated as follows:

$$\text{Biofilm change (\%)} = 1 - (\text{OD of tested compound treated cells})/(\text{OD of tested compound untreated cells}) \times 100.^{66}$$

3.3.4 Haemolytic activity. The hemolytic activity was assessed according to the method optimized by Gaspar and coworkers.[67,68] Ethylene diamine tetraacetic acid (EDTA), and preserved peripheral human blood obtained from voluntary donors were used on the same day for all experiments. Briefly, the erythrocytes were centrifugated at 1000×*g* for 10 min to separate them from the serum and washed three times in a PBS solution. The tested compound **29** and ciprofloxacin were prepared in PBS with a final concentration of 64 μg mL^{-1}. The assay was performed in 96-well plates in which 100 μL per well of sample were diluted with 100 μL of the erythrocyte suspension. The microplates were incubated at 37 °C for 1 h followed by centrifugation at 800×*g* for 10 min. The supernatant absorbance was measured at 570 nm with a reference filter at 600 nm. The percentage of hemolytic activity was calculated according to eqn (1):

$$\text{Hemolytic activity (\%)} = (\text{AbsS} - \text{AbsN}/\text{AbsP} - \text{AbsN}) \times 100 \quad (1)$$

where AbsS is the average absorbance of the sample, AbsN is the average absorbance of the negative control, and AbsP is the average absorbance of the positive control. All the compounds were tested in triplicate.

3.3.5 Growth curve analysis. The antibacterial efficacy was investigated using the growth-curve technique. Tests were conducted on compound **29** at 2 × MIC and 4 × MIC, and 1% DMSO was used as a control. Then, the bacteria were left to grow for a total of 0–3 h, 3–6 h, 9–12 h, 15–18 h, 21–24 h, and 24 h while shaking at 200 rpm at 37 °C. The optical density at 600 nm (OD600) of the supernatants was measured at many intervals using a UV-Vis spectrophotometer. For every item, three measurements were obtained in isolation. Using the above-described experiment, the exponential growth rate of MRSA was determined, plotting the optical density of the supernatant at 600 nm (OD600) along the vertical axis and time along the horizontal axis (ranging from 0 to 24 h).

3.3.6 SEM microscopic analysis. The antimicrobial action of the novel scaffold was illustrated using scanning electron microscopy (SEM).[65] The most active fractions were mixed with 0.5 McFarland standard of bacterial cells, and incubated for 14 h in nutrient broth at 37 °C and 120 rpm. Untreated bacteria are used as a control. For investigating the antimicrobial effect of new compound **29**, all the treated and untreated cells were harvested by centrifugation and washed three times with 0.1 M sodium phosphate buffer solution (pH 7.2). For SEM observation, a thin film of cells was smeared on a silver stub. The samples were gold-covered by cathodic spraying (Polaron gold). The morphology of the cells was observed on a scanning electron microscope (Jeol JSM-5400LV, USA). The SEM observation was carried out under the following analytical conditions: EHT = 20.00 kV, WD = 9.5 mm, and signal A = SE1.[69,70]

3.4. Molecular docking and binding data studies

PBP2a from methicillin-resistant *Staphylococcus aureus* (PDB ID: 1MWT) was used for docking simulations when covalently bound to the PNAM drug. The newly synthesized compound **29** was docked into the active site of the ATP-pocket of the 1MWT complex.[71] Re-docking studies were performed for the crystal structure 1MWT as a validation method. AutoDock tools[72] were used to process the enzyme. PyRx[73] was used to perform the docking. Discovery Studio Visualizer[74] was used to visualize and access the docking results. The AutoDock Tools package was employed to generate the docking input files and to analyze the docking results. A grid box size of 90 × 90 × 90 points with a spacing of 0.375 Å between the grid points was generated that covered almost the entire protein surface. Ligands were built by means of the AutoDock builder interface, and their geometries were optimized with the CHARMM forcefield[75] and then prepared for docking calculations with the Python scripts available in the Autodock package. For each ligand 50 runs were performed, and the resulting poses were clustered with 1.8 Å tolerance. Lamarckian GA was used for the conformational space search with an initial population set to 150, and fitness function evaluations set to 25, 000, 000. The most abundant low energy clusters were selected for analysis.[76–80]

Data availability

The data supporting this article have been included in the main manuscript and ESI.†

Author contributions

I confirm that the contributory role of each author listed in the article is shown below and some authors may have contributed to multiple roles. I am responsible for ensuring that the descriptions are accurate and agreed by all authors in this work. M. A. S.: synthesis and adjustment of methodology, spectroscopic analysis, and writing original draft. H. E. A. A.: conceptualization, supervision, molecular modelling, writing paper and review, and project administration. All authors have read and agreed to the published version of the manuscript. E. H. E. and A. T. A. B.: conceptualization, supervision, methodology, and writing original draft. M. A.: Molecular modeling and contribution to biochemical data evaluation and discussion, writing, review and editing, and funding acquisition. A. K. A. and S. S.: biological evaluation of target compounds, data analysis, and partial funding acquisition. M. R. A. and A. A.: writing proposal, supervision, synthesis, and partial funding acquisition.

Conflicts of interest

The authors declare that they have no competing interests. No financial support was received for this work. All authors have contributed significantly to the conception, design, execution, analysis, and interpretation of the work. All authors have reviewed and approved the final manuscript.

Acknowledgements

The authors extend their appreciation to the Deanship of Research and Graduate Studies at King Khalid University for funding this work through Large Research Project under grant number RGP2/346/45.

References

1 C. J. Murray, K. S. Ikuta, F. Sharara, L. Swetschinski, G. R. Aguilar, A. Gray, *et al.*, Global burden of bacterial antimicrobial resistance in 2019: a systematic analysis, *Lancet*, 2022, **399**(10325), 629–655.
2 T. Thompson, The staggering death toll of drug-resistant bacteria, *Nature*, 2022, DOI: **10.1038/d41586-022-00228-x**.
3 P. Hawkey, The growing burden of antimicrobial resistance, *J. Antimicrob. Chemother.*, 2008, **62**(suppl_1), i1–i9.
4 S. W. Long, *The Ongoing Threat of Methicillin-Resistant Staphylococcus aureus*, Oxford University Press US, 2020, pp. 1943–1945.
5 G. M. Rossolini, F. Arena, P. Pecile and S. Pollini, Update on the antibiotic resistance crisis, *Curr. Opin. Pharmacol.*, 2014, **18**, 56–60.
6 W. C. Reygaert, An overview of the antimicrobial resistance mechanisms of bacteria, *AIMS Microbiol.*, 2018, **4**(3), 482.
7 G. Cornaglia, *Fighting Infections Due to Multidrug-Resistant Gram-Positive Pathogens*, Elsevier, 2009, pp. 209–211.
8 J. Dai, R. Han, Y. Xu, N. Li, J. Wang and W. Dan, Recent progress of antibacterial natural products: Future antibiotics candidates, *Bioorg. Chem.*, 2020, **101**, 103922.
9 M. M. Elsebaei, H. Mohammad, M. Abouf, N. S. Abutaleb, Y. A. Hegazy, A. Ghiaty, *et al.*, Alkynyl-containing phenylthiazoles: Systemically active antibacterial agents effective against methicillin-resistant Staphylococcus aureus (MRSA), *Eur. J. Med. Chem.*, 2018, **148**, 195–209.
10 M. M. Elsebaei, N. S. Abutaleb, A. A. Mahgoub, D. Li, M. Hagras, H. Mohammad, *et al.*, Phenylthiazoles with nitrogenous side chain: an approach to overcome molecular obesity, *Eur. J. Med. Chem.*, 2019, **182**, 111593.
11 M. M. Elsebaei, H. Mohammad, A. Samir, N. S. Abutaleb, A. B. Norvil, A. R. Michie, *et al.*, Lipophilic efficient phenylthiazoles with potent undecaprenyl pyrophosphatase inhibitory activity, *Eur. J. Med. Chem.*, 2019, **175**, 49–62.
12 Y. Hosny, N. S. Abutaleb, M. Omara, M. Alhashimi, M. M. Elsebaei, H. S. Elzahabi, *et al.*, Modifying the lipophilic part of phenylthiazole antibiotics to control their drug-likeness, *Eur. J. Med. Chem.*, 2020, **185**, 111830.
13 A. Mancy, N. S. Abutaleb, M. M. Elsebaei, A. Y. Saad, A. Kotb, A. O. Ali, *et al.*, Balancing physicochemical properties of phenylthiazole compounds with antibacterial potency by modifying the lipophilic side chain, *ACS Infect. Dis.*, 2019, **6**(1), 80–90.
14 I. Eid, M. M. Elsebaei, H. Mohammad, M. Hagras, C. E. Peters, Y. A. Hegazy, *et al.*, Arylthiazole antibiotics targeting intracellular methicillin-resistant Staphylococcus aureus (MRSA) that interfere with bacterial cell wall synthesis, *Eur. J. Med. Chem.*, 2017, **139**, 665–673.
15 M. M. Elsebaie, H. T. N. El-Din, N. S. Abutaleb, A. A. Abuelkhir, H.-W. Liang, A. S. Attia, *et al.*, Exploring the structure-activity relationships of diphenylurea as an antibacterial scaffold active against methicillin-and vancomycin-resistant Staphylococcus aureus, *Eur. J. Med. Chem.*, 2022, **234**, 114204.
16 A. M. Helal, A. M. Sayed, M. Omara, M. M. Elsebaei and A. S. Mayhoub, Peptidoglycan pathways: there are still more, *RSC Adv.*, 2019, **9**(48), 28171–28185.
17 A. M. Sayed, N. S. Abutaleb, A. Kotb, H. G. Ezzat, M. N. Seleem, A. S. Mayhoub, *et al.*, Arylpyrazole as selective anti-enterococci; synthesis and biological evaluation of novel derivatives for their antimicrobial efficacy, *J. Heterocycl. Chem.*, 2023, **60**(1), 134–144.
18 I. G. Shahin, K. O. Mohamed, A. T. Taher, M. M. Elsebaei, A. S. Mayhoub, A. E. Kassab, *et al.*, New Phenylthiazoles: Design, Synthesis, and Biological Evaluation as Antibacterial, Antifungal, and Anti-COVID-19 Candidates, *Chem. Biodiversity*, 2023, **20**(11), e202301143.
19 A. Mancy, Synthesis and evaluation of antimicrobial activity of arylazole derivatives, *Al-Azhar J. Pharm. Sci.*, 2019, **60**(2), 43–50.

20 M. ElAwamy, H. Mohammad, A. Hussien, N. S. Abutaleb, M. Hagras, R. A. T. Serya, *et al.*, Alkoxyphenylthiazoles with broad-spectrum activity against multidrug-resistant gram-positive bacterial pathogens, *Eur. J. Med. Chem.*, 2018, **152**, 318–328.

21 M. M. Elsebaei, N. S. Abutaleb, A. A. Mahgoub, D. Li, M. Hagras, H. Mohammad, *et al.*, Phenylthiazoles with nitrogenous side chain: An approach to overcome molecular obesity, *Eur. J. Med. Chem.*, 2019, **182**, 111593.

22 M. M. Elsebaei, H. Mohammad, M. Abouf, N. S. Abutaleb, Y. A. Hegazy, A. Ghiaty, *et al.*, Alkynyl-containing phenylthiazoles: Systemically active antibacterial agents effective against methicillin-resistant Staphylococcus aureus (MRSA), *Eur. J. Med. Chem.*, 2018, **148**, 195–209.

23 A. Hammad, N. S. Abutaleb, M. M. Elsebaei, A. B. Norvil, M. Alswah and A. O. Ali, From phenylthiazoles to phenylpyrazoles: broadening the antibacterial spectrum toward carbapenem-resistant bacteria, *J. Med. Chem.*, 2019, **62**(17), 7998–8010.

24 I. Eid, M. M. Elsebaei, H. Mohammad, M. Hagras, C. E. Peters, Y. A. Hegazy, *et al.*, Arylthiazole antibiotics targeting intracellular methicillin-resistant Staphylococcus aureus (MRSA) that interfere with bacterial cell wall synthesis, *Eur. J. Med. Chem.*, 2017, **139**, 665–673.

25 A. Hammad, N. S. Abutaleb, M. M. Elsebaei, A. B. Norvil, M. Alswah, A. O. Ali, *et al.*, From phenylthiazoles to phenylpyrazoles: broadening the antibacterial spectrum toward carbapenem-resistant bacteria, *J. Med. Chem.*, 2019, **62**(17), 7998–8010.

26 Y.-W. He, C.-Z. Dong, J.-Y. Zhao, L.-L. Ma, Y.-H. Li and H. A. Aisa, 1, 2, 3-Triazole-containing derivatives of rupestonic acid: click-chemical synthesis and antiviral activities against influenza viruses, *Eur. J. Med. Chem.*, 2014, **76**, 245–255.

27 S. Ulloora, R. Shabaraya and A. V. Adhikari, Facile synthesis of new imidazo [1, 2-a] pyridines carrying 1, 2, 3-triazoles via click chemistry and their antiepileptic studies, *Bioorg. Med. Chem. Lett.*, 2013, **23**(11), 3368–3372.

28 S. N. Darandale, N. A. Mulla, D. N. Pansare, J. N. Sangshetti and D. B. Shinde, A novel amalgamation of 1, 2, 3-triazoles, piperidines and thieno pyridine rings and evaluation of their antifungal activity, *Eur. J. Med. Chem.*, 2013, **65**, 527–532.

29 A. Kamal, S. M. A. Hussaini, S. Faazil, Y. Poornachandra, G. N. Reddy, C. G. Kumar, *et al.*, Anti-tubercular agents. Part 8: synthesis, antibacterial and antitubercular activity of 5-nitrofuran based 1, 2, 3-triazoles, *Bioorg. Med. Chem. Lett.*, 2013, **23**(24), 6842–6846.

30 C. Kaushik, K. Lal, A. Kumar and S. Kumar, Synthesis and biological evaluation of amino acid-linked 1, 2, 3-bistriazole conjugates as potential antimicrobial agents, *Med. Chem. Res.*, 2014, **23**, 2995–3004.

31 Y. Dürüst, H. Karakuş, M. Kaiser and D. Tasdemir, Synthesis and anti-protozoal activity of novel dihydropyrrolo [3, 4-d][1, 2, 3] triazoles, *Eur. J. Med. Chem.*, 2012, **48**, 296–304.

32 M. F. Mady, G. E. Awad and K. B. Jørgensen, Ultrasound-assisted synthesis of novel 1, 2, 3-triazoles coupled diaryl sulfone moieties by the CuAAC reaction, and biological evaluation of them as antioxidant and antimicrobial agents, *Eur. J. Med. Chem.*, 2014, **84**, 433–443.

33 W. Zhang, Z. Li, M. Zhou, F. Wu, X. Hou, H. Luo, *et al.*, Synthesis and biological evaluation of 4-(1, 2, 3-triazol-1-yl) coumarin derivatives as potential antitumor agents, *Bioorg. Med. Chem. Lett.*, 2014, **24**(3), 799–807.

34 Y. Yang, B. A. Rasmussen and D. M. Shlaes, Class A β-lactamases—enzyme-inhibitor interactions and resistance, *Pharmacol. Therapeut.*, 1999, **83**(2), 141–151.

35 A. J. Weinstein, The cephalosporins: activity and clinical use, *Drugs*, 1980, **20**(2), 137–154.

36 E. Perucca, J. Cloyd, D. Critchley and E. Fuseau, Rufinamide: clinical pharmacokinetics and concentration–response relationships in patients with epilepsy, *Epilepsia*, 2008, **49**(7), 1123–1141.

37 S. B. Ötvös, Á. Georgiádes, I. M. Mándity, L. Kiss and F. Fülöp, Efficient continuous-flow synthesis of novel 1, 2, 3-triazole-substituted β-aminocyclohexanecarboxylic acid derivatives with gram-scale production, *Beilstein J. Org. Chem.*, 2013, **9**(1), 1508–1516.

38 S. Sonoda, T. Yamaguchi, K. Aoki, D. Ono, A. Sato, C. Kajiwara, *et al.*, Evidence of latent molecular diversity determining the virulence of community-associated MRSA USA300 clones in mice, *Immun., Inflammation Dis.*, 2018, **6**(3), 402–412.

39 I. A. Tickler, R. V. Goering, J. R. Mediavilla, B. N. Kreiswirth, F. C. Tenover and H. A. I. Consortium, Continued expansion of USA300-like methicillin-resistant Staphylococcus aureus (MRSA) among hospitalized patients in the United States, *Diagn. Microbiol. Infect. Dis.*, 2017, **88**(4), 342–347.

40 C. B. Long, R. P. Madan and B. C. Herold, Diagnosis and management of community-associated MRSA infections in children, *Expert Rev. Anti.*, 2010, **8**(2), 183–195.

41 B. Wang, B. Pachaiyappan, J. D. Gruber, M. G. Schmidt, Y. M. Zhang and P. M. Woster, Antibacterial Diamines Targeting Bacterial Membranes, *J. Med. Chem.*, 2016, **59**(7), 3140–3151.

42 P. S. Stewart, Mechanisms of antibiotic resistance in bacterial biofilms, *Int. J. Med. Microbiol.*, 2002, **292**(2), 107–113.

43 A. Gristina, Biomaterial-centered infection: microbial adhesion versus tissue integration. 1987, *Clin. Orthop. Relat. Res.*, 2004, **427**, 4–12.

44 A. G. Gristina, Biomaterial-centered infection: microbial adhesion versus tissue integration, *Science*, 1987, **237**(4822), 1588–1595.

45 European Medicines Agency, *Guideline on Strategies to Identify and Mitigate Risks for First-In-Human and Early Clinical Trials with Investigational Medicinal Products; EMEA/CHMP/SWP/28367/07 Rev. 1; Committee for Medicinal Products for Human Use (CHMP)*, Amsterdam, The Netherlands, 2017.

46 H. Mohammad, H. E. Eldesouky, T. Hazbun, A. S. Mayhoub and M. N. Seleem, Identification of a Phenylthiazole Small Molecule with Dual Antifungal and Antibiofilm Activity Against Candida albicans and Candida auris, *Sci. Rep.*, 2019, **9**(1), 18941.

47 A. Hammad, N. S. Abutaleb, M. M. Elsebaei, A. B. Norvil, M. Alswah, A. O. Ali, *et al.*, From Phenylthiazoles to Phenylpyrazoles: Broadening the Antibacterial Spectrum toward Carbapenem-Resistant Bacteria, *J. Med. Chem.*, 2019, **62**(17), 7998–8010.

48 M. A. Seleem, A. M. Disouky, H. Mohammad, T. M. Abdelghany, A. S. Mancy, S. A. Bayoumi, *et al.*, Second-Generation Phenylthiazole Antibiotics with Enhanced Pharmacokinetic Properties, *J. Med. Chem.*, 2016, **59**(10), 4900–4912.

49 M. M. Elsebaie, H. T. Nour El-Din, N. S. Abutaleb, A. A. Abuelkhir, H.-W. Liang, A. S. Attia, *et al.*, Exploring the structure-activity relationships of diphenylurea as an antibacterial scaffold active against methicillin- and vancomycin-resistant Staphylococcus aureus, *Eur. J. Med. Chem.*, 2022, **234**, 114204.

50 G. Muteeb, M. T. Rehman, M. Shahwan and M. Aatif, Origin of Antibiotics and Antibiotic Resistance, and Their Impacts on Drug Development: A Narrative Review, *Pharmaceuticals*, 2023, **16**(11).

51 L. L. Silver, Challenges of antibacterial discovery, *Clin. Microbiol. Rev.*, 2011, **24**(1), 71–109.

52 N. Lv, Q. Kong, H. Zhang and J. Li, Discovery of novel Staphylococcus aureus penicillin binding protein 2a inhibitors by multistep virtual screening and biological evaluation, *Bioorg. Med. Chem. Lett.*, 2021, **41**, 128001.

53 T. A. Łeski and A. Tomasz, Role of penicillin-binding protein 2 (PBP2) in the antibiotic susceptibility and cell wall cross-linking of Staphylococcus aureus: evidence for the cooperative functioning of PBP2, PBP4, and PBP2A, *J. Bacteriol.*, 2005, **187**(5), 1815–1824.

54 R. Lipp, The Innovator Pipeline: Bioavailability Challenges and Advanced Oral Drug Delivery Opportunities, **http://www.americanpharmaceuticalreview.com/Featured-Articles/135982-The-Innovator-Pipeline-Bioavailability-Challenges-and-Advanced-Oral-Drug-Delivery-Opportunities**, 2013 May 11, 2017 [cited 2013.

55 H. Mohammad, A. S. Mayhoub, A. Ghafoor, M. Soofi, R. A. Alajlouni, M. Cushman, *et al.*, Discovery and characterization of potent thiazoles versus methicillin- and vancomycin-resistant Staphylococcus aureus, *J. Med. Chem.*, 2014, **57**(4), 1609–1615.

56 S. Kumar, A. S. Pathania, N. K. Satti, P. Dutt, N. Sharma, F. A. Mallik, *et al.*, Synthetic modification of hydroxychavicol by Mannich reaction and alkyne–azide cycloaddition derivatives depicting cytotoxic potential, *Eur. J. Med. Chem.*, 2015, **92**, 236–245.

57 J. An, G. Y. Zuo, X. Y. Hao, G. C. Wang and Z. S. Li, Antibacterial and synergy of a flavanonol rhamnoside with antibiotics against clinical isolates of methicillin-resistant Staphylococcus aureus (MRSA), *Phytomedicine : international journal of phytotherapy and phytopharmacology*, 2011, **18**(11), 990–993.

58 N. Rezki, S. A. Al-Sodies, H. E. A. Ahmed, S. Ihmaid, M. Messali, S. Ahmed, *et al.*, A novel dicationic ionic liquids encompassing pyridinium hydrazone-phenoxy conjugates as antimicrobial agents targeting diverse high resistant microbial strains, *J. Mol. Liq.*, 2019, **284**, 431–444.

59 I. Wiegand, K. Hilpert and R. E. Hancock, Agar and broth dilution methods to determine the minimal inhibitory concentration (MIC) of antimicrobial substances, *Nat. Protoc.*, 2008, **3**(2), 163–175.

60 T. Mosmann, Rapid colorimetric assay for cellular growth and survival: application to proliferation and cytotoxicity assays, *J. Immunol. Methods*, 1983, **65**(1–2), 55–63.

61 F. Demirci and K. H. C. Başer, Bioassay Techniques for Drug Development By Atta-ur-Rahman, M. Iqbal Choudhary (HEJRIC, University of Karachi, Pakistan), William J. Thomsen (Areana Pharmaceuticals, San Diego, CA). Harwood Academic Publishers, Amsterdam, The Netherlands. 2001. xii + 223 pp. 15.5 × 23.5 cm. $79.00. ISBN 90-5823-051-1, *J. Nat. Prod.*, 2002, **65**(7), 1086–1087.

62 G. A. O'Toole, Microtiter dish biofilm formation assay, *J. Vis. Exp.*, 2011, **47**.

63 K. Alam, D. A. A. Farraj, E. F. S. Mah, M. A. Yameen, M. S. Elshikh, R. M. Alkufeidy, *et al.*, Anti-biofilm activity of plant derived extracts against infectious pathogen-Pseudomonas aeruginosa PAO1, *J. Infect. Public. Health.*, 2020, **13**(11), 1734–1741.

64 H. E. A. Ahmed, H. A. Abdel-Salam and S. MAJBc, Synthesis, characterization, molecular modeling, and potential antimicrobial and anticancer activities of novel 2-aminoisoindoline-1,3-Dione derivatives, *Bioorg. Chem.*, 2016, **66**, 1–11.

65 A. M. Omar, S. Ihmaid, E. E. Habib, S. S. Althagfan, S. Ahmed, H. S. Abulkhair, *et al.*, The rational design, synthesis, and antimicrobial investigation of 2-Amino-4-Methylthiazole analogues inhibitors of GlcN-6-P synthase, *Bioorg. Chem.*, 2020, **99**, 103781.

66 A. Hend, El-sayed YAF. Correlation between biofilm formation and multidrug resistance in clinical isolates of Pseudomonas aeruginosa, *Microbes and Infectious Diseases*, 2021, **2**(3), 541–549.

67 J. C. Bastos, N. S. M. Vieira, M. M. Gaspar, A. B. Pereiro and J. M. M. Araújo, Human Cytotoxicity, Hemolytic Activity, Anti-Inflammatory Activity and Aqueous Solubility of Ibuprofen-Based Ionic Liquids, *Sustainable Chem.*, 2022, **3**(3), 358–375.

68 M. M. Gaspar, S. Calado, J. Pereira, H. Ferronha, I. Correia, H. Castro, *et al.*, Targeted delivery of paromomycin in murine infectious diseases through association to nano lipid systems, *Nanomed. Nanotechnol. Biol. Med.*, 2015, **11**(7), 1851–1860.

69 F. M. War Nongkhlaw and S. R. Joshi, Microscopic study on colonization and antimicrobial property of endophytic bacteria associated with ethnomedicinal plants of Meghalaya, *J. Microsc. Ultrastruct.*, 2017, **5**(3), 132–139.

70 B. Sarkar, B. K. Dey, M. Sarkar and S. J. Kim, A smart production system with an autonomation technology and dual channel retailing, *Computers & Industrial Engineering*, 2022, **173**, 108607.

71 S. Howard, V. Berdini, J. A. Boulstridge, M. G. Carr, D. M. Cross, J. Curry, *et al.*, Fragment-Based Discovery of

the Pyrazol-4-yl Urea (AT9283), a Multitargeted Kinase Inhibitor with Potent Aurora Kinase Activity, *J. Med. Chem.*, 2009, **52**(2), 379–388.

72 G. M. Morris, D. S. Goodsell, R. S. Halliday, R. Huey, W. E. Hart, R. K. Belew, *et al.*, Automated docking using a Lamarckian genetic algorithm and an empirical binding free energy function, *J. Comput. Chem.*, 1998, **19**(14), 1639–1662.

73 S. Dallakyan and A. J. Olson, Small-molecule library screening by docking with PyRx, *Methods in Molecular Biology (Clifton, NJ)*, 2015, vol. 1263, 243–250.

74 M. A. Soliman, H. E. Ahmed, E. H. Eltamany, A. T. Boraei, A. Aljuhani, S. A. Salama, *et al.*, Novel bis-benzimidazole-triazole hybrids: anticancer study, in silico approaches, and mechanistic investigation, *Future Med. Chem.*, 2024, 1–15.

75 K. Vanommeslaeghe, E. Hatcher, C. Acharya, S. Kundu, S. Zhong, J. Shim, *et al.*, CHARMM general force field: A force field for drug-like molecules compatible with the CHARMM all-atom additive biological force fields, *J. Comput. Chem.*, 2010, **31**(4), 671–690.

76 A. A. Awaji, W. A. Z. E. Zaloa, M. A. Seleem, M. Alswah, M. M. Elsebaei, A. H. Bayoumi, *et al.*, N- and s-substituted Pyrazolopyrimidines: A promising new class of potent c-Src kinase inhibitors with prominent antitumor activity, *Bioorg. Chem.*, 2024, **145**, 107228.

77 A. M. E. A. Malebari, H. Ahmed, S. K. Ihmaid, A. M. Omar, Y. A. Muhammad, S. S. Althagfan, *et al.*, Exploring the dual effect of novel 1,4-diarylpyranopyrazoles as antiviral and anti-inflammatory for the management of SARS-CoV-2 and associated inflammatory symptoms, *Bioorg. Chem.*, 2023, **130**, 106255.

78 M. T. Khayat, H. E. A. Ahmed, A. M. Omar, Y. A. Muhammad, K. A. Mohammad, A. M. Malebari, *et al.*, A novel class of phenylpyrazolone-sulphonamides rigid synthetic anticancer molecules selectively inhibit the isoform IX of carbonic anhydrases guided by molecular docking and orbital analyses, *J. Biomol. Struct. Dyn.*, 2023, 1–19.

79 M. Almaghrabi, A. Musa, A. K. B. Aljohani, H. E. A. Ahmed, M. Alsulaimany, S. F. Miski, *et al.*, Introducing of novel class of pyrano[2,3-c]pyrazole-5-carbonitrile analogs with potent antimicrobial activity, DNA gyrase inhibition, and prominent pharmacokinetic and CNS toxicity profiles supported by molecular dynamic simulation, *J. Biomol. Struct. Dyn.*, 2023, 1–18.

80 M. Alsehli, A. Aljuhani, S. K. Ihmaid, S. M. El-Messery, D. I. A. Othman, A.-A. A. A. El-Sayed, *et al.*, Design and Synthesis of Benzene Homologues Tethered with 1,2,4-Triazole and 1,3,4-Thiadiazole Motifs Revealing Dual MCF-7/HepG2 Cytotoxic Activity with Prominent Selectivity via Histone Demethylase LSD1 Inhibitory Effect, *Int. J. Mol. Sci.*, 2022, **23**(15), 8796.